Infrared Spectroscopy of Discrete Uranyl Anion Complexes

Gary S Groenewold, Anita K Gianotto, Michael E Mcilwain, Michael J van Stipdonk, Michael Kullman, Travis J. Cooper, David T Moore, Nick Polfer, Jos Oomens, Ivan Infante, et al.

Infrared Spectroscopy of Discrete Uranyl Anion Complexes

Gary S. Groenewold, Anita K. Gianotto, and Michael E. McIlwain*

Idaho National Laboratory, Idaho Falls, ID, USA

Michael J. Van Stipdonk, Michael Kullman, and Travis J. Cooper*

Wichita State University, Wichita, KS, USA

David T. Moore, Nick Polfer, and Jos Oomens

FOM Instituut voor Plasmafysica Rijnhuizen, Nieuwegein, The Netherlands.

Ivan Infante, Lucas Visscher

Vrije Universiteit Amsterdam, The Netherlands

Bertrand Siboulet

DEN/DRCP/SCPS, CEA Marcoule, 30207, Bagnols-sur-Cèze cedex, France

Wibe A. de Jong

Pacific Northwest National Laboratory, Richland, WA, USA

AUTHOR ADDRESS: Idaho National Laboratory, P. O. Box 1625, Idaho Falls, ID 83415-2208

AUTHOR EMAIL ADDRESS: gary.groenewold@inl.gov

RECEIVED DATE (automatically inserted by publisher);

TITLE RUNNING HEAD: Discrete Uranyl Anion Complexes

ABSTRACT: The Free-Electron Laser for Infrared Experiments (FELIX) was used to study the wavelength-resolved multiple photon dissociation of discrete, gas phase uranyl (UO_2^{2+}) complexes containing a single anionic ligand (A), with or without ligated solvent molecules (S). The uranyl antisymmetric and symmetric stretching frequencies were measured for complexes with general formula $[UO_2A(S)_n]^+$, where A was either hydroxide, methoxide, or acetate; S was water, ammonia, acetone, or acetonitrile; and n = 0-3. The values for the antisymmetric stretching frequency for uranyl ligated with only an anion ($[UO_2A]^+$) were as low or lower than measurements for $[UO_2]^{2+}$ ligated with as many as five strong neutral donor ligands, and are comparable to solution phase values. This result was surprising because initial DFT calculations predicted values that were 30–40 cm^{-1} higher, consistent with intuition but not with the data. Modification of the basis sets and use of alternative functionals improved computational accuracy for the methoxide and acetate complexes, but calculated values for the hydroxide were greater than the measurement regardless of the computational method used. Attachment of a neutral donor ligand S to $[UO_2A]^+$ produced $[UO_2AS]^+$, which produced in only very modest changes to the uranyl antisymmetric stretch frequency, and did not universally shift the frequency to lower values. DFT calculations for $[UO_2AS]^+$ were in accord with trends in the data, and showed that attachment of the solvent was accommodated by weakening of the U-anion bond as well as the uranyl. When uranyl frequencies were compared for $[UO_2AS]^+$ species having different solvent neutrals, values decreased with increasing neutral nucleophilicity.

KEYWORDS: IRMPD, DFT, actinide, free electron laser, coordination complex, mass spectrometry

INTRODUCTION

The chemical behavior of uranium in general, and the linear uranyl dication $[UO_2]^{2+}$ in particular, is diverse on account of the relative ease of redox processes,[1] and the availability of f and d orbitals[2-4] for complex formation. The latter has a profound affect on the solubility of the element.[5,6] In solution, $[UO_2]^{2+}$ is the dominant species,[6-8] where it plays an important role in heavy element separations[9] and in mobility of the element in the environment.[10] At low pH, $[UO_2]^{2+}$ exists as the solvated dication in solution with weakly complexing anions.[10] Hydrolysis[11,12] at higher solution pH values, or the presence of more strongly coordinating anions, produces uranyl complexes coordinated by one or more anionic ligands.[8,13]

The chemical diversity of species has motivated research in vibrational spectroscopy and computational chemistry to understand the coordination and nature of bonding in uranyl complexes containing different ligands because these factors have reactivity and stability implications.[14,15] Infrared and Raman spectroscopy studies of $[UO_2]^{2+}$ have shown that the respective antisymmetric (ν_3) and symmetric (ν_1) stretching frequencies[16] act as convenient "thermometers" for gauging the electron-donating capability of the equatorial ligand field, because the frequencies are strongly correlated with the coordination environment. Nucleophilic ligands in the coordination sphere donate electron density to the cationic metal center, and this spills over into the π^*-antibonding orbitals of the uranyl ion to cause a concomitant decrease in the associated ν_1 and ν_3 frequencies. Increased electron density at the uranium metal center can be effected by attachment of more donor ligands,[17] or by increasing the nucleophilicity of the ligands.[18,19] Generally for a modestly complexing solution environment, ν_3 values near 960 cm^{-1} are typical,[18] as originally reported by Jones and Penneman in 1953.[20] However, when more strongly basic ligands like hydroxide[7,12,21,22] are present, the resulting complexes exhibit much lower ν_3 values, which have been noted in both solutions[23,24] and solids.[25-28] Similar trends for the symmetric ν_1 stretch are seen in Raman spectra[12,15,29] and strong correlations between ν_1 and ν_3 frequencies have been

established.[30] Increasing the local electron density at the metal center in other ways, such as by formal reduction (to UO_2^+)[24,31] or substitution of a more electron-rich metal (i.e. Np, Pu, Am), produces a similar effect.[29,32]

Computational chemistry[2,3] helps provide a quantitative understanding of structure and bonding in uranyl complexes. Impressive progress has been made using density functional theory (DFT),[33-36] which is remarkable given the theoretical difficulty of accounting for the large number of electrons, spin-orbit coupling, and relativistic effects encountered in modeling uranyl molecules.[33,35] The computational results are strongly influenced by the choice of functional, basis set and effective core potential employed.[37,38] Vibrational frequencies generated using DFT[37,39,40] are invaluable because they provide a basis for the interpretation of spectroscopy experiments. However, comparisons between theory and, for example, solution-phase experimental studies are complicated because multiple species may be present in solution[8,41] as a result of rapid ligand exchange, ion pair formation, redox reactions, and solvent effects.[1,7,11,12,17,42] Because vibrational spectra collected from solution-phase experiments potentially contain contributions from multiple species, comparisons to results produced by DFT calculations (which are generated for discrete, well-defined species) are difficult. Longer-range interactions with the second solvation sphere also influence the spectroscopy of the complexes, and further complicate comparisons. An elegant way around this is to compare DFT results to structures determined using X-ray crystallography, however the effect of neighboring molecules in the crystal lattice is a complicating factor.[43]

An alternative approach for converging vibrational spectroscopy and computational chemistry is to measure the infrared spectra of discrete species isolated in the gas phase,[44] which can be accomplished using a trapped ion mass spectrometer (MS) (e.g., a Fourier transform ion cyclotron resonance [FT-ICR] or quadrupole ion trap instrument) interfaced to a high intensity, tunable infrared source that is provided by a free electron laser.[41,44-47] Using electrospray ionization (ESI),[48-51] a wide range of UO_2^{2+} species[52-55] can be formed and isolated in the FT-ICR-MS. Normally, ion concentrations in the gas phase are too

low to enable direct absorption measurements, but by rapid absorption of 10s to 100s of photons, the vibrational energy of a discrete species may be raised to the point where bond cleavage occurs.[44,56] In this case, photon absorption is signaled by a change in ion mass, and plotting ion intensities as a function of wavelength produces infrared multiple photon dissociation (IRMPD) spectra which bear strong similarity to those measured using conventional absorption approaches.[57-59]

In prior research campaigns, the IRMPD strategy was used to produce spectra of discrete uranyl-solvent complexes $[UO_2S_{n=2-5}]^{2+}$ where S = acetone (ACO) and or acetonitrile (ACN).[60] The uranyl ν_3 frequency underwent systematic red shifts with serial addition of donor ligands, and with substitution of a stronger nucleophilic ligand for a weaker one (e.g. ACO for ACN). Interestingly, the uranyl ν_3 frequencies measured using IRMPD were never as low as the value for UO_2^{2+} in solution,[20] despite the fact that the ligands in the gas-phase experiments (ACO and ACN) were stronger nucleophiles than H_2O (the dominant ligand in solution). This observation led to conjecture that additional interactions may be contributing to the observed uranyl shift in solution-phase experiments.

The subject of this report is the IRMPD spectroscopy of gas-phase $[UO_2A]^+$ species (where anion A = OH, OCH_3, and acetate (OAc)), and complexes in which $[UO_2A]^+$ is modified by the attachment of a single neutral donor solvent S, to form $[UO_2AS_{1-2}]^+$ (where S = H_2O, NH_3, ACN, or ACO). The hydroxide and acetate anions are representative of those commonly encountered in solution-phase studies of UO_2^{2+} speciation,[61] and acetate and methoxide are models for functional groups expected to interact with UO_2^{2+} in biological and geochemical environments. The primary focus of this work is to explore and understand the trends in the antisymmetric uranyl stretching frequency (ν_3), as a function of the number and binding strength of the various anionic and neutral ligands, by comparing the experimental IRMPD results with predictions from electronic structure calculations employing several different computational methods. In general, the measured ν_3 frequencies for the bare anion complexes were significantly lower than the predicted computational values, and approached those measured in solution for coordinatively saturated UO_2^{2+}. Addition of a neutral donor to form $[UO_2AS]^+$ did not

substantially alter the ν_3 values compared to $[UO_2A]^+$, which was surprising because prior studies showed that the antisymmetric stretch is systematically red-shifted upon attachment of a donor neutral ligand. Comparison of the ν_3 values for different $[UO_2AS]^+$ complexes showed a systematic decrease with increasing nucleophilicity of the neutral donor S. DFT calculations also suggested that when the neutral is added bonding is accommodated by weakening both the uranyl-anion bond, as well as the uranyl moiety.

EXPERIMENTAL

IRMPD spectra were collected at the Free Electron Laser for Infrared eXperiments (FELIX) facility, located at the FOM Instituut voor Plasmafysica 'Rijnhuizen' (Nieuwegein, The Netherlands).[47] The free electron laser is interfaced to a custom-built Fourier transform ion cyclotron resonance (FT-ICR) mass spectrometer.[57,62]

Generation of Uranyl Complexes by Electrospray Ionization (ESI). ESI was used to generate singly- and doubly-charged uranyl complexes.[52,54] A one millimolar solution of uranyl nitrate was generated by dissolving the hexahydrate salt (Fluka/Sigma-Aldrich, St. Louis, MO, USA) in water to produce uranyl complexes that were introduced into the hexapole ion accumulation chamber. The ESI source (Micromass, Manchester, U.K.) was operated at 3 kV with respect to ground. Ions were generated at atmospheric pressure and were extracted into vacuum using ion optics oriented orthogonally with respect to the spray axis, and then gated into a hexapole ion accumulation chamber where they were stored for 0.5–1.0 s prior to being transmitted into the FT-ICR-MS. The mass spectra observed were sensitive to various temperatures, voltages and carrier-gas and solution flow rates of the ESI source. Particularly important were the desolvation temperature[54] (which was controlled by a heater and thermocouple on the block through which the spray capillary passed) and the temperature of the desolvation gas, which were maintained at 29 and 52^{o}C, respectively. The flow rate of the spray solution was 25 μl min^{-1}, and the desolvation gas (N_2, which ensheathed the solution spray) flow rate was

maintained at 30 L min^{-1}. Attempts to make hydrated $[UO_2NO_3]^+$ were not successful because traces of methanol, acetone, acetonitrile, acetic acid and ammonia in the spray chamber resulted in production of hydroxide, methoxide and acetate complexes. By increasing the radio frequency power on the ion accumulation hexapole, most of the ion population was converted to $[UO_2OH]^+$, $[UO_2OCH_3]^+$ and $[UO_2OAc]^+$; these species were also formed as complexes with a single solvent molecule (see below), which provided the ensemble of species for infrared spectroscopy.

Fourier Transform Ion Cyclotron Resonance Mass Spectrometry (FT-ICR-MS), and Infrared Multiphoton Dissociation (IRMPD).[46,57,59] Ions accumulated in the external hexapole were gated into the ICR cell, where complexes identified for IRMPD were isolated using a stored waveform inverse Fourier transform (SWIFT) pulse.[63] This ejected all species except those having the desired mass. Isolated ionic complexes were irradiated using two FELIX macropulses, which induced elimination of a solvent molecule, a radical or a rearrangement product (depending on the complex) when the incident wavelength matched an absorption band. The IRMPD mechanism has been described in detail elsewhere.[45,62,64] Briefly, it involves sequential, non-coherent absorption of many (tens to hundreds) infrared photons, with each photon being "relaxed" by intramolecular vibrational redistribution (IVR) before the next one is absorbed. In this way, the internal vibrational energy of the molecule can be resonantly increased above the dissociation threshold, resulting in fragmentation. It has been shown that the infrared spectra obtained are comparable to those obtained using linear absorption techniques.[56,65] FELIX (60 mJ per macropulse, 5 μs pulse duration, bandwidth 0.2 – 0.5 % of central λ) was scanned primarily through the spectral region of interest around 10 μm, in increments $\leq$ 0.04 μm, after which IRMPD product ions and un-dissociated precursor ions were measured using the excite/detect sequence of the FT-ICR-MS.[66,67] The IRMPD efficiency was then expressed as –log(1-[summed fragment ion yield]), corrected for the width of the acquisition channels and linearly normalized to correct for variations in FELIX power over the spectral range. Peak centers were chosen by fitting a Gaussian peak to the data using Origin plotting software(version 7.5, OriginLab, Northampton, MA). Precision was

not evaluated, on account of the time required for repetitive acquisition of the peak profiles, and the precious nature of beam time at FELIX. Nevertheless, the precision of measurement of peak position is probably on the order of a couple of cm^{-1}, based on earlier examination of the position(s) of the antisymmetric uranyl stretch and carbonyl C=O stretch in double charged complexes.[60]

Because some of the complexes were difficult to fragment, signal-to-noise was less than desired, and so the isolated complexes were subjected to multiple irradiation/acquisition sequences at each wavelength across the scanned region. This lengthened acquisition time, and this factor together with the need to strictly economize beam time at the FELIX FT-ICR-MS beamline constrained data acquisition for most complexes to the diagnostic O=U=O antisymmetric stretch (ν_3).

Density Functional Theory (DFT) Structure and Frequency Calculations. DFT calculations were performed using several different approaches, which varied in treatment of relativistic and core polarization effects, functional, basis set, and software package used. This was done to compare approaches that are commonly available and executable by non-specialists with more advanced methodologies that require access to substantial computational power.

(1) Calculations using local density approximation (LDA) with the Vosko, Wilk and Nusair (VWN) parameterization[68,69] were performed using the Accelrys Inc. DMol^3 suite.[70,71] This approach was employed because these calculations could be readily executed and provided an instant theoretical feedback on the recorded spectra. This efficiency is in large part due to use of a semi-core pseudopotential[72] was applied to describe the core electrons, combined with the use of polarized numerical basis sets (DNP) for the active electrons. A fine (10^{-8}) energy convergence criterion was employed to ensure optimal geometries and representative vibrational frequencies. With this approach it was possible to calculate most structures in only a few hours using eight processors. No scaling of the calculated frequencies was performed.

(2) DFT calculations of structures and harmonic frequencies with the more accurate hybrid B3LYP functional[73,74] were performed with the NWChem[75,76] and Gaussian[77] suite of programs. Different

combinations of functionals and basis sets were employed in efforts to derive a consistent view of the IRMPD phenomena measured in the context of complex structure and dissociation behavior. Uranium was described by an effective core potential and its associated basis set: either the LANL2dz ECP and orbital basis set[78] or the MWB60 ECP and basis set (SDD),[83-86] which features Stuttgart/Dresden effective core potentials were used for uranium. Other atoms in the complexes (O, C, H, and N) were described using the aug-cc-pVDZ orbital basis sets,[79] the D95V basis set,[83-86] the all-electron 3-21g* basis sets, or the 6-31+g(d) basis set. The relatively small 3-21g basis (which include single first polarization functions on row 2 atoms) set is generally considered to be too small for use in modeling actinide molecules, but one goal of this study was to evaluate the use of the SDD/3-21g* general basis set approach for interpretation of gas-phase IRMPD experiments.

(3) In addition NWChem was used to perform correlation corrected vibrational self consistent field (cc-VSCF) calculations[80-82] that provide an estimate of the effect of anharmonicity and mode-coupling for the fundamental vibrational states. Starting with the vibrational self-consistent field (VSCF) method, degenerate perturbation theory is used to correct for effects of correlation between different vibrational modes, enabling calculation of anharmonic vibrational states for polyatomic molecules.

(4) Finally we also employed the ADF2006.01[87] package to quantitatively assess the donation of the ligands to the uranyl moiety and to compute the energetic requirements for different dissociation channels. Prior experience indicated reliable thermodynamic accuracy and thus motivated this approach. Geometric parameters (structures and frequencies) were thereby determined at the scalar relativistic ZORA[88]-PW91[89]-TZ2P level of theory using a restricted DFT and a small frozen core, while fragmentation energies were computed including spin-orbit coupling terms. The charge transfer between ligands and the uranyl was analyzed using both Hirshfeld charge analysis and Voronoi Deformation Density (VDD) methods. The energy differences reported do not reflect energies to transition states (which may be relevant for the loss of H_2O from $[UO_2OH(ACO)]^+$ and photo-fragmentation of $[UO_2OCH_3]^+$).

RESULTS AND DISCUSSION

IRMPD of Uranyl-Hydroxide Complexes $[UO_2OH]^+$. Electrospray ionization mass spectrometry of aqueous uranyl nitrate solutions modified with organic solvents had previously been shown to produce dications ligated with neutral donors, provided the capillary temperature was kept close to ambient.[54,60] However, by modestly increasing the capillary temperature and the RF power of the ion accumulation hexapole, uranyl ion pairs were formed that enabled examination of their IRMPD spectra, as a complement to prior measurements made for the uranyl dication bound with neutral ligands.[60] A prominent $[UO_2OH]^+$ ion was produced at *m/z* 287, and lower abundance complexes were observed at *m/z* 345, 328, 305 and 304 that correspond to $[UO_2OH(ACO)]^+$, $[UO_2OH(ACN)]^+$, $[UO_2OH(H_2O)]^+$and $[UO_2OH(NH_3)]^+$, respectively. The ammonia, acetone, and acetonitrile were present in the hexapole accumulation region of the ESI/FT-ICR instrument from prior experiments that involved the use of the solvents and ammonium acetate buffer solutions. The five different hydroxide complexes that were furnished by manipulation of the electrospray conditions were isolated using a SWIFT sequence,[67] and then photo-fragmented by scanning the free electron laser over the spectral region corresponding to the uranyl antisymmetric stretching frequency (~ 1000 cm^{-1}); the resulting IRMPD spectra are shown in Figure 1.

Photo-fragmentation of $[UO_2OH]^+$ resulted in reductive elimination of a hydroxyl radical, and the antisymmetric uranyl ν_3 stretch for this species appeared as a broadened absorption centered at 971 cm^{-1} (Figure 1). The low abundance and profile of the peak reflected inefficient photo-fragmentation and high energetic requirements:[44] Calculations using ZORA-PW91-TZ2P (*vide infra*) indicated that the energy to dissociate the complex to $[UO_2]^+$ and a hydroxyl radical was 96.4 kcal mol^{-1}. The ν_3 value for $[UO_2OH]^+$ was lower than the most red-shifted dication complexes $[UO_2(ACO)_4]^{2+}$ (988 cm^{-1}) and $[UO_2(ACN)_5]^{2+}$ (995cm^{-1}), which suggested at first glance that a single hydroxide transfers as much or more electron density to the uranium center as does four or five strong donors in a fully coordinated uranyl complex. This conclusion was surprising, and in fact opposed the results of VDD analyses, that

indicated a charge transfer of 0.52 e from the hydroxide to the uranyl, while the charge transfer from four acetones accounted for 0.62 e.

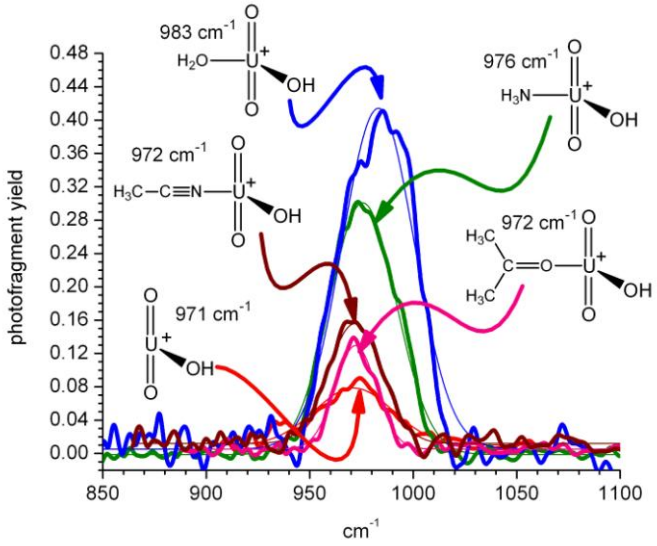

Figure 1. Infrared multiple photon dissociation spectra of the antisymmetric O=U=O stretching region for $[UO_2OH]^+$ and ligand complexes containing (clockwise) a single ACN, H_2O, NH_3, and ACO. The yield values for the ACN complex were multiplied by a factor of two, to visually distinguished it from the unmodified hydroxide complex.

The value for the $[UO_2OH]^+$ uranyl antisymmetric stretching frequency was lower than anticipated based on prior DFT calculations using B3LYP. A red shift of 183 cm^{-1} was calculated for $[UO_2(OH)_2]$ by Marsden and coworkers;[40] subtraction of this value from 1140 cm^{-1} (the value calculated for unligated $[UO_2]^{2+}$)[38] produces a frequency of 957 cm^{-1} for the bis-hydroxy complex. The measured value of 971 cm^{-1} for the monohydroxy cannot be compared directly, because the modeled and measured complexes are different. But the values are reasonably close to each other, which suggests that most of the red shift results from attachment of the first OH^- ligand, and that attachment of the second ligand

produces a much more modest change in frequency. This trend is in qualitative agreement with very small shifts produced by attachment of neutral donors to $[UO_2A]^+$ complexes (*vide infra*).

The $[UO_2OH]^+$ ν_3 value measured in the gas phase is very close to that measured in aqueous solution for $[UO_2]^{2+}$ (960 to 965 cm^{-1}), which is considered to have five inner sphere aquo ligands.[17,18,20,90,91] Lower values have been measured for hydroxide complexes in solution, but these have been attributed to species having multiple uranyl moieties, e.g. a ν_3 measurement at ~ 940 cm^{-1} has been assigned to $[(UO_2)_2(OH)_2]^{2+}$,[17,21,92] and an even lower ν_3 value of 923 cm^{-1} to $[(UO_2)_3(OH)_5]^+$.[17,92] These ν_3 measurements indicate that the frequency is decreased by the presence of more than one U atom in the complexes, but are also certainly influenced by coordinated solvent molecules.

The appearance of $[UO_2OH]^+$ complexed with one or more solvent molecules enabled the effect of neutral donor ligands on the antisymmetric stretching frequency to be examined. The prior study of $[UO_2]^{2+}$ complexes with neutral ligands[60] showed that the antisymmetric stretching frequency was sequentially red-shifted by the serial attachment of additional neutral donor ligands, for example in the acetone (ACO) complexes $[UO_2(ACO)_n]^{2+}$, the frequency decreased from 1017 to 1000 to 988 cm^{-1} as n went from 2 to 3 to 4 (respectively).[60] The trend measured for a series of acetonitrile (ACN) complexes was similar, as was the magnitude of the red shift caused by an additional donor neutral. These observations led to the expectation that attachment of a neutral donor to $[UO_2OH]^+$ would result in a similar red shift.

Isolation and photo-fragmentation of $[UO_2OH(ACO)]^+$ resulted in parallel elimination reactions: loss of intact ACO, and loss of H_2O (Scheme 1, Table 1). Computationally, the two pathways were found to have very similar reaction energies: using ZORA-PW91-TZ2P both channels were endothermic by 41.4 kcal/mol, and a similar conclusion was derived using B3LYP/LANL2dz/aug-cc-pVDZ, which predicted values of 46.5 and 42.6 kcal/mol for loss of ACO and H_2O respectively. The loss of H_2O involves transfer of a proton from a methyl carbon on ACO to the hydroxide, leaving behind the acetone enolate which calculations show remains coordinated through the oxygen atom. No difference in frequencies

was observed in the two photo-fragment channels, which had maxima at 972 cm^{-1}. This value was effectively equal to the measurement for the unmodified $[UO_2OH]^+$, which initially would seem to indicate that addition of the strong ACO donor had no further effect on the uranyl moiety. However, this conclusion is inconsistent with the fairly strong binding predicted by the PW91 and B3LYP calculations. Furthermore, the carbonyl stretching region for the $[UO_2OH(ACO)]^+$ complex was scanned and an absorption with a value of 1633 cm^{-1} was found. In our previous study of $[UO_2(ACO)_n]^{2+}$ complexes, we observed that the ligand CO stretch was strongly red-shifted to 1515 cm^{-1} in the n=2 complex, and that this shift decreased with increasing cluster size, to 1583 for n=3 and 1630 for n=4, as the binding energy per ligand was reduced.[60,93] Thus based on this comparison of carbonyl stretching data, one would expect the binding of the ACO ligand in the $[UO_2OH(ACO)]^+$ complex to be comparable to binding in the $[UO_2(ACO)_4]^{2+}$ complex. Interestingly, addition of a second and third ACO ligand to $[UO_2OH(ACO)]^+$ produced red-shifts consistent with the prior experiments. Photo-fragmentation of $[UO_2OH(ACO)_2]^+$ and $[UO_2OH(ACO)_3]^+$ both resulted in the loss of an ACO, with a ν_3 of 961 and 948 cm^{-1} respectively. Therefore, a red-shift of 11 and 13 cm^{-1} were observed on going from $[UO_2OH(ACO)]^+$ $[UO_2OH(ACO)_2]^+$ to $[UO_2OH(ACO)]^+$, which agrees well with the magnitude of the red-shifts resulting from ACO addition to the $[UO_2(ACO)_n]^{2+}$ complexes.[60] Taken together, these results suggest that it may be the uranyl antisymmetric stretching frequency in the bare $[UO_2OH]^+$ complex that is anomalously shifted, which is certainly possible given the particular susceptibility of this very small system to anharmonicity effects arising from the IRMPD mechanism. These anharmonicity effects are examined in more detail below.

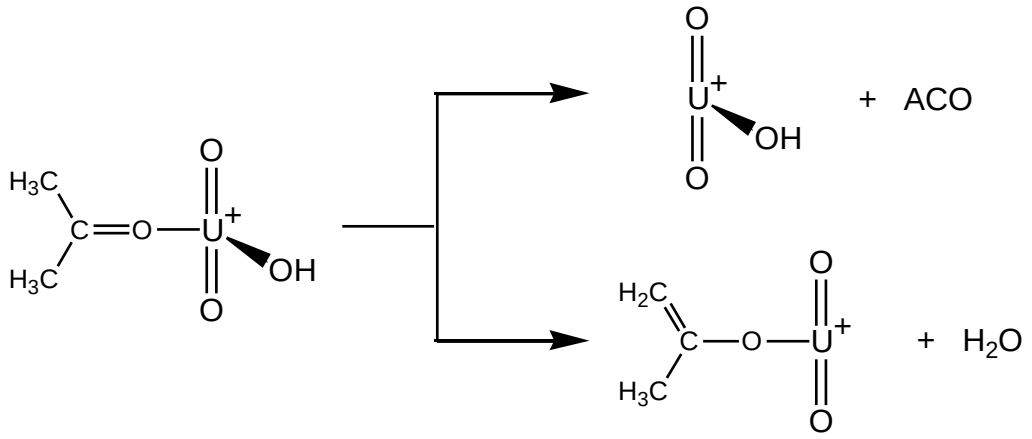

Scheme 1. Parallel elimination reactions of isolation and photo-fragmentation of $[UO_2OH(ACO)]^+$.

Table 1. Dissoication energies for IRMPD reactions of $[UO_2OH(ACO)]^+$ calculated using different basis sets.

Reaction / binding energy (kcal/mol)	B3LYP SVWN Stuttgart RSC TZVP NWChem	B3LYP PW91 ZORA TZ2P (ADF)
$[UO_2OH(ACO)]^+ \rightarrow [UO_2OH]^+ + ACO$	48.3	41.4
$[UO_2OH(ACO)]^+ \rightarrow [UO_2(OC_3H_5)]^+ + H_2O$	52.8	41.4

Isolation of the $[UO_2OH(ACN)]^+$ complex followed by photo-fragmentation produced elimination of ACN. The antisymmetric UO_2 stretch was measured at 972 cm^{-1}, nearly identical to that for $[UO_2OH(ACO)]^+$ and to $[UO_2OH]^+$. The hydroxide complex with ammonia $[UO_2OH(NH_3)]^+$ underwent photo-fragmentation solely by loss of NH_3, with a ν_3 value at 976 cm^{-1}, which is slightly *blue* shifted compared to the unmodified uranyl hydroxide. The final hydroxide complex examined was $[UO_2OH(H_2O)]^+$, which eliminated H_2O upon irradiation that maximized at 983 cm^{-1}, which was 12 cm^{-1} higher than the $[UO_2OH]^+$ value.

The trend for the uranyl ν_3 frequencies for the $[UO_2OH(S)]^+$ complexes were internally self-consistent, i.e., they decreased in the order $H_2O > NH_3 > ACN \sim ACO > (ACO)_2$. These frequency values are inversely correlated with the calculated coordination energies of different S molecules,[40] and are in accord with comparisons of ACO and ACN uranyl complexes.[60] The observed ordering again highlights the remarkably low value measured for unmodified $[UO_2OH]^+$, which would be expected to be higher than 983 cm^{-1} (i.e., the value for the complex with the most weakly bound neutral, $[UO_2OH(H_2O)]^+$). Because it does not seem reasonable to expect that the addition of weakly donating species actually strengthens the uranyl U=O bonds, we must seek other explanations for the blue shifted bands for the NH_3 and H_2O complexes.

One likely contributing factor is vibrational anharmonicity derived from the multiple photon absorption process. Red-shifts in the spectra of the *para*-aminobenzoic acid[58] and $[CeOH(ACO)_3]^{2+}$ cations[93] have been attributed to IRMPD anharmonicity, and the same phenomenon may contribute to the low frequency measured for $[UO_2OH]^+$. These studies demonstrate that when molecules or complexes attain very high internal energies via the IRMPD process, their vibrational bands exhibit non-negligible red-shifts. This can be particularly dramatic for systems with low densities of states,[44] such as the $[UO_2OH]^+$ complex studied here, which only has 9 vibrational modes. The energy required to dissociate $[UO_2OH]^+$ to $[UO_2]^+$ and a hydroxyl radical was evaluated computationally, and both the Stuttgart RSC ECP and the ADF TZ2P basis sets, which have some similarity, produced high values (Table 2). However, a lower value was generated using the LANL/aug-cc-pvdz basis set, which may reflect that difficulty is encountered in dealing with $[UO_2]^+$ species using the LANL/aug-cc-pvdz basis set, which is fairly small, without any diffuse functions. This could conceivably create an unbalanced description of uranium, leading to a low calculated dissociation energies. Therefore, we conclude that the calculations in general predict high dissociation energies, which is consistent with the fact that hydroxide had the highest coordination energy of any ligand in the extensive compilation calculated by Marsden and coworkers.[40] These considerations support the attribution of the anomalously low

$[UO_2OH]^+$ ν_3 value to anharmonicity effects. The B3LYP calculations using the Stuttgart RSC/TZVP basis was also performed starting from a triplet excited state, and it was found to require 43.8 kcal mol^{-1}. This value, when added to the promotion energy (see below) yields a value of nearly 90 kcal mol^{-1}.

Table 2. Dissociation energies calculated for IRMPD of $[UO_2OH]^+$.

Reaction / binding energy (kcal/mol)	B3LYP SVWN Stuttgart RSC TZVP (NWChem)	B3LYP PW91 ZORA TZ2P (ADF)
$[UO_2OH]^+ \rightarrow [UO_2^+] + OH$ dissociation via a singlet ground state	74.5	96.0
$[UO_2OH]^+ \rightarrow [UO_2^+] + OH$ dissociation via a triplet excited state	43.8	--

In contrast to the small $[UO_2OH]^+$ molecule, more complex systems containing a neutral ligand tend to have reduced dissociation energies and a significantly higher vibrational density of states. For example, water binds to the $[UO_2OH]^+$ complex by only 30 kcal/mol, while doubling the number of vibrational modes, three of which are low-frequency intermolecular modes, that may contribute disproportionately to the vibrational density of states. This may explain why the ν_3 frequencies of the $[UO_2OH(S)]^+$ complexes are not apparently affected by anharmonicity, compared to the bare $[UO_2OH]^+$ which is strongly shifted by anharmonicity induced by the IRMPD process. A ν_3 value unshifted by anharmonicity would be expected to be ~990 cm^{-1} for $[UO_2OH]^+$ to be consistent with the trend in the ν_3 bands of the $[UO_2OH(S)]^+$ complexes measured here.

Correlation corrected vibrational SCF (cc-VSCF) calculations can provide an estimate of whether or not differential red-shifting would be expected in comparing $[UO_2OH]^+$ and $[UO_2OH(S)]^+$ complexes.

cc-VSCF estimates the effect of anharmonicity by including coupling between the lower vibrational modes calculated in the harmonic approximation. Factoring in an influence by anharmonicity the calculated ν_3 value for $[UO_2OH]^+$ decreased by 10 cm^{-1}, which would account for part of the expected red shift for the hydroxide based on the IRMPD data. However, the shift calculated for $[UO_2OH(H_2O)]^+$ was very nearly the same at 8 cm^{-1}, since there are other factors that are expected to mitigate the effects of anharmonicity in the latter system, the differential anharmonic shift calculated for $[UO_2OH]^+$ and $[UO_2OH(H_2O)]^+$. It should be noted that the cc-VSCF calculations only consider coupling of the lowest ~10 vibrational levels, whereas coupling and population of the higher excitation levels would certainly be expected to contribute at the high excitation energies achieved in the IRMPD experiments.

Participation of an electronically excited state $[UO_2OH]^+$ may also contribute to the apparently low ν_3 frequency. The energy calculated for promotion of an electron into the lowest excited triplet state calculated using both B3LYP/LANL2dz-aug-cc-pVDZ and PW91/unrestricted/scalar was ~45 kcal/mol, which was less than that calculated to dissociate $[UO_2OH]^+$ (except for the LANL basis set). If vibrational-to-electronic transitions are occurring in the multiple photon experiments, then a lowered frequency would be expected for the electronically excited molecule.[94] The ν_3 value calculated for $[UO_2OH]^+$ in its lowest excited state was quite a bit lower, at 908 cm^{-1}, however the hydroxide profile is broadened, which may be the result of overlap of absorptions of ground state and excited state molecules. It should also be noted that this triplet state may be directly related to the observed dissociation pathway, suggesting that the molecule can be considered to be a complex of reduced uranyl $[UO_2]^+$and neutral hydroxyl radical.

IRMPD of Uranyl-Acetate Complexes $[UO_2OAc]^+$. ESI produced a relatively abundant ion at *m/z* 329 which was attributed to uranyl acetate $[UO_2OAc]^+$, that was formed from residual acetic acid that had been used to enhance the protonated ion formation from peptide and protein solutions in previous experiments at FELIX. Because acetate is a stronger conjugate base, it replaces nitrate in the ion accumulation chamber prior to injection into the FT-ICR-MS. The composition was confirmed by

accurate mass measurement and the photo-fragmentation pathway observed in the IRMPD experiment, in which a neutral loss of 42 mass units (presumably as ketene) furnished $[UO_2OH]^+$ as the product ion. For IRMPD of $[UO_2OAc]^+$ the maximum for the antisymmetric uranyl stretch was 995 cm^{-1} (Figure 2), higher than any of the hydroxide complexes measured. This is consistent with the fact that acetate is a weaker gas-phase base[95] than either hydroxide or methoxide (vide infra), and consequently is also likely to be a weaker uranophile. Despite the presumed lower basicity, the antisymmetric uranyl stretching frequency for $[UO_2OAc]^+$ appeared at a lower value than nearly all of the uranyl dication complexes ligated with multiple neutral donor ligands reported earlier.[60] In solution, acetate complexes have been the subject of several infrared studies, and the most appropriate value for the antisymmetric stretch to use in a comparison is 954 cm^{-1}, which was measured by Quiles[17] for $[UO_2OAc]^+$. This value is significantly lower than the IRMPD measurement, which reflects the attachment of additional solvent ligands to the $[UO_2OAc]^+$ metal center. Other studies have produced values that ranged as low as 919 cm^{-1},[18,23] but these measurements probably contain contributions from species that contain more than one acetate ligand, and the possibility of variable acetate coordination.[17] Recently, LDA was used by de Jong and coworkers to calculate uranyl ν_3 value for $[UO_2OAc]^+$ at 1025 cm^{-1}.[96] A careful examination of the carbonyl stretching frequencies could provide insight into this, and will be investigated in further experimental campaigns.

Also observed in the ESI spectrum were low abundance ions at *m/z* 346 and 347 that corresponded to ammonia and water complexes (respectively), having compositions $[UO_2OAc(NH_3)]^+$ and $[UO_2OAc(H_2O)]^+$. Photo-fragmentation of these complexes involved elimination of either NH_3 or H_2O, producing $[UO_2OAc]^+$ in each case. Consistent with prior studies of donors, the antisymmetric UO_2 stretching frequency was red-shifted for both H_2O and NH_3 complexes relative to $[UO_2OAc]^+$, although the magnitude of the shifts were small: the value for the H_2O complex at 993 cm^{-1} was lower by 2 cm^{-1}, while a shift 7 cm^{-1} to 988 cm^{-1} was observed for the NH_3 complex. The trend in the measured frequencies indicate that both H_2O and NH_3 are donating electron density, and that NH_3 is a stronger

uranophile than is H_2O, consistent with Marsden's prior DFT results,[40] the relative order of proton affinities,[95] and bonding to other metal cations.[97] The fact that the frequency of the unmodified acetate is very close to that of both ligand complexes suggests that the frequency for the $[UO_2OAc]^+$ complex may also be red-shifted as a result of anharmonicity or perhaps other factors. However the effect is less pronounced than in the case of the hydroxide complex, as indicated by the fact that the ν_3 of the unmodified $[UO_2OAc]^+$ complex is not lower than the values of the H_2O and NH_3 adducts. Compared to the hydroxide complex, a smaller anharmonic red shift for OAc is consistent with a higher density of states,[44] and with a lower energy requirement for fragmentation of the acetate complex, which involves rearrangement rather than direct bond-cleavage and elimination of a radical.

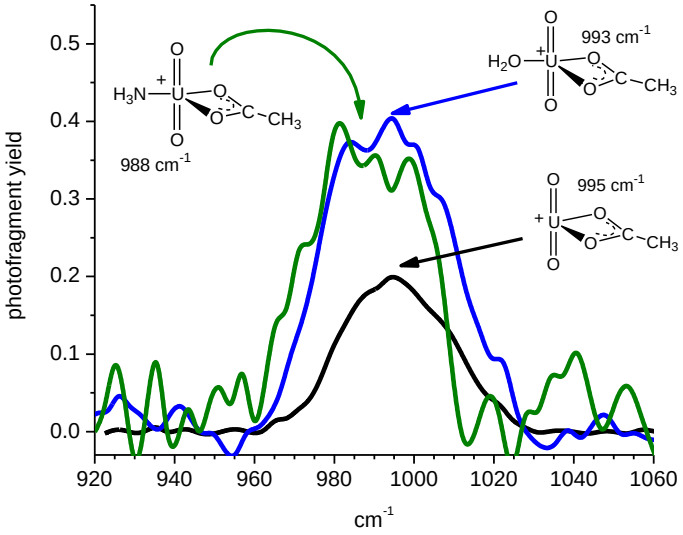

Figure 2. Infrared multiple photon dissociation spectra of the antisymmetric O=U=O stretching region for $[UO_2OAc]^+$ and ligand complexes containing a single NH_3 and H_2O.

IRMPD of Uranyl-Methoxide Complexes $[UO_2OCH_3]^+$. The accurate mass measurement of the ion at *m/z* 301 confirmed the composition of uranyl methoxide, which was formed by reaction of uranyl species with methanol that was present in the ESI solution. Photo-fragmentation of $[UO_2OCH_3]^+$ produced four different product ions corresponding to the elimination of the OCH_3 and H radicals, H_2, and H_2CO (Scheme 2).

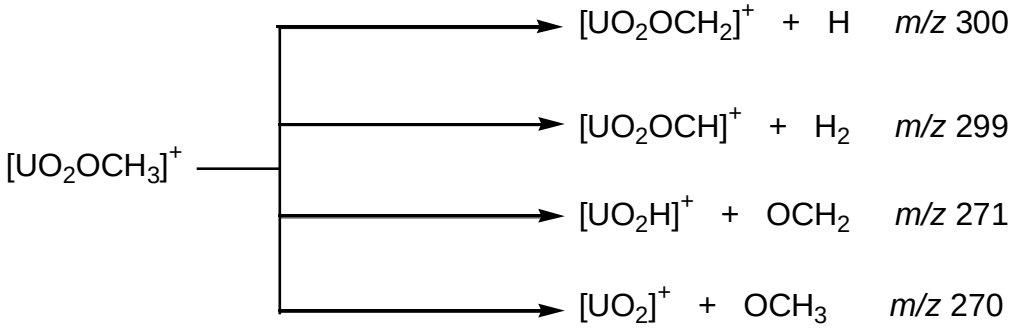

Scheme 2: Photo-fragmentation of $[UO_2OCH_3]^+$ produced four different product ions corresponding to the elimination of the OCH_3 and H radicals, H_2, and H_2CO.

The IRMPD spectrum of the methoxide complex contained two bands, with maxima at 975 cm^{-1} and 887 cm^{-1} (Figure 3, black trace). DFT calculations (B3LYP/SDD-3-21G*) indicated that the higher frequency corresponded to overlapped antisymmetric uranyl ν_3 and C-O stretching bands, and the lower frequency to the symmetric uranyl ν_1 band normally observed in the Raman spectrum.[7,12,15,22,29] The appearance of the symmetric stretch indicates a lowered symmetry in the complex, resulting from strong binding of the methoxide that perturbs the linearity of the uranyl functional group. This was supported by the lowest energy structures and bond angles produced by B3LYP calculations (vide infra).

Striking differences were observed when the IR spectra produced using the different photo-dissociation channels were compared. The spectrum generated by monitoring the loss of the OCH_3 radical contained a single sharply defined peak with a maximum at 967 cm^{-1}, a frequency slightly lower than that measured for the uranyl antisymmetric stretch for the unmodified hydroxide complex, and consistent with the fact that methoxide is a stronger base than is hydroxide. The peak centered at 967 cm^{-1} was not observed in the spectra generated by the other three fragmentation channels, either because it is not occurring in these channels, or because it was overlapped with the O-C stretch (see below). If the latter is true, then it suggests that the ν_3 frequency in the spectrum of the OCH_3 loss channel is red shifted by about 20 cm^{-1} due to the higher energetic requirements for that channel; shifts of this magnitude have been observed previously.[58]

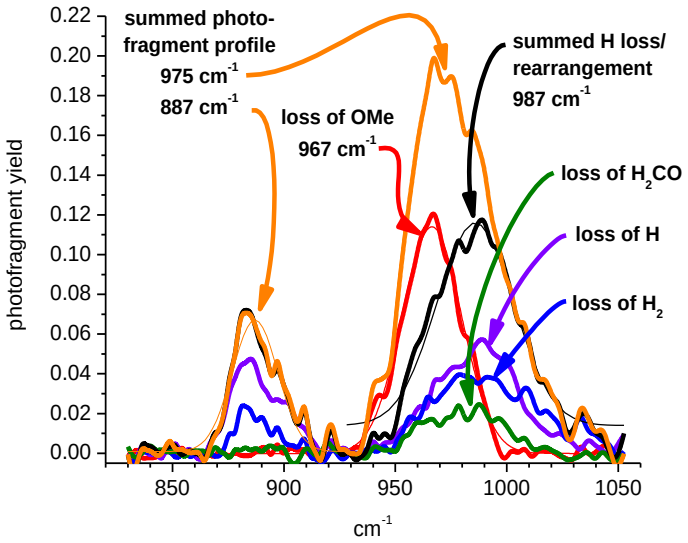

Figure 3. Infrared multiple photon dissociation spectra of the symmetric and antisymmetric O=U=O ν_3 stretching region for $[UO_2OCH_3]^+$. The black trace represents the spectrum generated by the summed photofragment abundance; red the OCH_3 radical elimination, violet the H radical elimination; blue the H_2 elimination; green the H_2CO elimination, and orange the sum of the H loss/rearrangement related channels.

The IR spectra generated from the photo-dissociation channels corresponding to either the loss of H or H_2 bore strong similarities to one another in that they contained a peak with a maximum at 987 cm^{-1} and second peak at about 887 cm^{-1}. The higher frequency peak probably contains components from unresolved uranyl asymmetric stretch and C-O stretching, while the lower frequency peak corresponds to the symmetric UO_2 stretch. The IR spectrum generated by the H_2CO elimination was similar to the H-loss spectra, but lacked the band for the symmetric stretch. The appearance of very dissimilar IR spectra in the different photo-dissociation channels was remarkable, because IRMPD spectra generated from competing mass channels are normally identical or are very similar, with the fragmentation channels having the higher energetic requirements being modestly red-shifted as a result of anharmonicity that results from population of higher vibrational levels when multiple photons are serially absorbed.[58,93] Fast intramolecular vibrational redistribution randomizes the deposited energy regardless of the

frequency of initial deposition, and thus the competing fragmentation channels display similar if not identical IR spectra.[56]

A hypothetical interpretation of these observations is that the order of reaction endothermicities for the four reactions is $-H_2 \sim -H < -OCH_2 < -OCH_3$. In the spectra generated by losses of H and H_2 peaks are seen in all three absorption modes, symmetric uranyl, asymmetric uranyl and C-O (assuming that the asymmetric uranyl and C-O are overlapping). The symmetric uranyl and C-O are weakly absorbing modes and hence are only seen in those eliminations having low energy requirements. The spectrum generated by loss of OCH_2 contains the asymmetric uranyl and perhaps the C-O, but energetic requirement for this channel is too high to enable observation of the symmetric uranyl stretch. The higher energetic requirements are probably related to the fact that the $[UO_2H]^+$ product ion has to be reduced, forming either a U(IV) species or a uranyl hydride. Finally, the spectrum generated by loss of OCH_3 contains only the antisymmetric uranyl peak, because the energetics for this reaction are higher, which means that it can only be accessed via the high intensity ν_3 uranyl absorption. This peak is substantially red-shifted as a consequence of the large number of photons that must be deposited in order for the reaction to occur. Further, the fast kinetics of the OCH_3 radical loss reduces observation of the slower, lower energy losses.

Enthalpy changes for the calculated for the different fragmentation channels display modest agreement with this hypothesis. B3LYP calculations using different parameterization and basis sets (Table 3) showed that elimination of H_2 was the lowest, followed by loss of H radical. Enthalpy requirements for the loss of H_2CO and reductive elimination of the methoxy radical were higher, and the order of these two varied depending on the basis sets employed. The B3LYP calculations identified two possible outcomes for the elimination of H_2CO: formation of a U(IV) oxyhydroxide $[UOOH]^+$, and a U(VI) uranyl hydride $[UO_2H]^+$, with the U(IV) species appearing to be somewhat disfavored energetically. However the significant energetic variations seen in comparisons of the different approaches do not allow us to state the energetic order of the elimination reactions, and thus computational support is

somewhat equivocal for the hypothetical explanation for the differences seen in the spectra from the four elimination channels.

Table 3. Calculated enthalpies for the dissociation reactions of $[UO_2OCH_3]^+$ (Scheme 2). Values are in kcal mol^{-1}.

Reaction \ binding energy (kcal/mol)	?????? SVWN DNP DNP (DMOL)	B3LYP B3LYP SDD SDD (Gaussian)	B3LYP SVWN Stuttgart RSC TZVP (NWChem)	B3LYP PW91 ZORA TZ2P (ADF)*
$[UO_2OCH_3]+ \rightarrow H_2 + [UO_2(OCH)]^+$		52.8	52.7	52.3
$[UO_2OCH_3]+ \rightarrow H + [UO_2(OCH_2)]^+$		67.3	73.7	78.3
$[UO_2OCH_3]+ \rightarrow OCH_3 + [UO_2]^+$		68.4	69.8	100.1
$[UO_2OCH_3]+ \rightarrow OCH_2 + [UO_2(H)]^+$ (H equatorial)		59.0	80.7	--
$[UO_2\text{-}OCH_3]+ \rightarrow OCH_2 + [UOOH]^+$ (H linear)		79.9	85.2	85.6

* ZORA numbers include spin-orbit interaction.

An alternative explanation would be the existence of two or more isomers of $[UO_2OCH_3]^+$, however DFT calculations did not support the existence of energetically competitive isomers, although rearrangement may be occurring during the IRMPD process. An alternative structure that was considered contained an H atom bound to uranium, with formaldehyde equatorially coordinated: for such a structure an absoption corresponding to carbonyl group should be observed, but a survey of the 1500–1700 cm^{-1} wavelength region did not show an additional peak. Thus a structure involving a bound formaldehyde ligand is unlikely, as our prior studies[60,93] showed that the C=O stretch can be readily detected in complexes with carbonyl-containing ligands.

Involvement of an excited state for the uranyl methoxide can also be argued, which would be expected to have energetic requirements similar to the 45 kcal/mol required for the hydroxide complex. Intuitively, this is an attractive explanation because a higher spin species would be expected to have a higher propensity for rearrangement and elimination of H and OCH_3 radicals. When the energetic

requirement for conversion to a triplet excited state was calculated, it was found to be 45 kcal mol^{-1}, in a range that would be accessible during the IRMPD photofragmentation. However, as in the two previously offered rationalizations, this too remains speculative at the present time, and hence an unequivocal identification of the origin of the differences in the spectra of the different mass channels is still elusive.

The assignment of the higher frequency to a C-O stretch drew support from the spectra acquired for the $[UO_2OCH_3(H_2O)]^+$ and $[UO_2OCH_3(NH_3)]^+$ adducts (Figure 4). The three peaks in the spectra of these complexes had frequencies consistent with the spectra of unmodified $[UO_2OCH_3]^+$. In the adduct ions, photo-fragmentation of the methoxide ligand did not occur; instead, only the energetically favored losses of H_2O or NH_3 were observed.

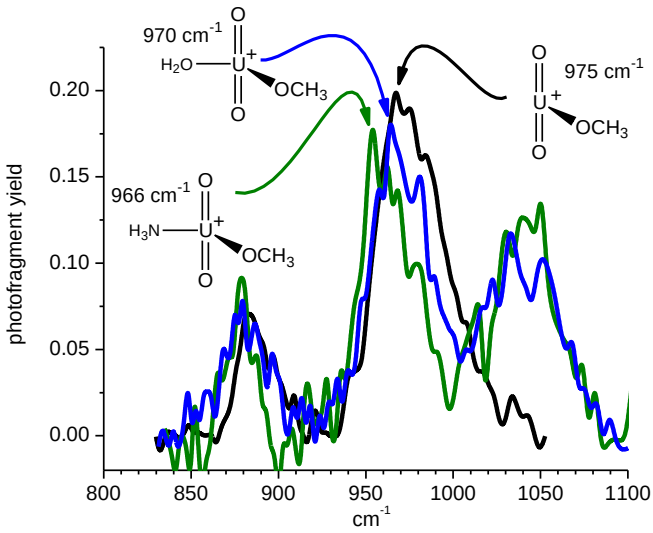

Figure 4. Infrared multiple photon dissociation spectra of the antisymmetric O=U=O stretching region for $[UO_2OCH_3]^+$ (black trace, sum of all photo-fragment channels), $[UO_2OCH_3(H_2O)]^+$ (blue trace, scaled by 0.55) and $[UO_2OCH_3(NH_3)]^+$ (green trace scaled by 0.6). The photofragment yield for the H_2O and NH_3 complexes was higher than for the unmodified methoxide complex, and scaling was performed to facilitate comparison.

The frequencies measured for the antisymmetric UO_2 stretch for the H_2O and NH_3 complexes were modestly red-shifted compared to the maximum value for the summed photo-fragment channels of the unmodified $[UO_2OCH_3]^+$, and the trend observed is consistent with what would be expected for addition of a second weak donor ligand (H_2O), and then substitution of a slightly more basic ligand NH_3 for H_2O. Similarly, the frequencies measured for the symmetric stretch were very similar for all three complexes: the ν_1 value for the unmodified $[UO_2OCH_3]^+$ was measured at 887 cm^{-1}, and the peak position is only very modestly shifted to 880 cm^{-1} when H_2O is attached, and to 879 cm^{-1} for NH_3. These values are about 20 cm^{-1} higher than that measured for solvated $[UO_2OAc]^+$ using Raman spectroscopy.[12] As in the case of the hydroxide complexes, the uranyl stretching frequencies of the methoxide complexes were not significantly red shifted by addition of a neutral donor ligand. This suggests that in the unmodified methoxide complex $[UO_2OCH_3]^+$, the uranyl frequency may be shifted to a lower value as a result of anharmonicity, in a fashion similar to that suspected to be occurring in the hydroxide complexes. As noted, this would be facilitated by high energetic requirements for the elimination reaction in the unmodified $[UO_2OCH_3]^+$ which was indicated by calculations, and was comparable to the value calculated for the hydroxide. The high value is consistent with the idea that elimination of the OCH_3 radical would be most susceptible to red-shifting resulting from absorption of multiple photons during the IRMPD process.

While addition of a second donor ligand does not cause large changes in the uranyl stretching frequencies,[43,96] it appears to strengthen the C-O bond in the methoxide ligand. This would be expected if the methoxide were modestly repelled by attachment of H_2O or NH_3 to the uranium center. In the spectra for both $[UO_2OCH_3(H_2O)]^+$ and $[UO_2OCH_3(NH_3)]^+$, the C-O stretch was observed at ca. 1038 and 1040 cm^{-1}, shifted to higher frequency by ~ 50 cm^{-1} compared to unmodified $[UO_2OCH_3]^+$. This trend is directly analogous to what was observed in the IR spectra of discrete uranyl acetone dication complexes: when an additional donor ligand was added, the binding of all equatorial ligands was weakened, and the C=O stretching frequency increased, approaching that of free acetone;[60] in the

present case, it is the C-O stretch of methoxide that is increased. Calculations also suggested loosening of the U-OCH_3 bond upon ligation with a neutral donor.

Comparisons of Calculated Frequencies

The changes in vibrational frequencies can be understood in part by comparison with frequencies, bond lengths and angles calculated using density functional theory. Because calculations of complexes containing actinide elements are challenging, different combinations of functionals and basis sets were used. These results provided multiple opportunities for comparison with measurements, in particular using the antisymmetric uranyl stretch, which was the salient figure of merit in this study. A comparison of the unscaled uranyl frequencies calculated using B3LYP with different basis sets versus the IRMPD measurements (Figure 5, Table 4) showed that more accurate values were obtained using the SDD basis set for all elements. Calculated values using 3-21g* and 6-31+g(d) for C, H, N and O were 20 – 30 cm^{-1} higher than measurements for the solvent complexes, depending on the donor. Values calculated using 6-31+g(d) were slightly better than those generated using 3-21g*, but differences between the two calculations were small. The data in Figure 5 may be grouped into three categories: anion complexes with no donor, an O-donor (H_2O or acetone), or an N-donor (NH_3 or acetonitrile). Calculations for the O-donor anion complexes were in best agreement with experiments, being within a few cm^{-1} for the all-SDD basis sets, and on the order of 20 cm^{-1} high for the SDD/3-21g* and SDD/6-31+g(d) basis sets. Calculations for the complexes containing a neutral that coordinates via a N atom were slightly less accurate, with differences ranging from 5 – 10 cm^{-1} for the all-SDD calculation to ~ 30 cm^{-1} using the gen basis sets. This suggests that N-donation is slightly more aggressive in the gas phase experiment than predicted by theory. Calculations for the $[UO_2(anion)]^+$ complexes containing no neutral donor displayed the poorest agreement with experiment, being 20 to nearly 60 cm^{-1} higher than the measurements, depending on the basis set used. The poorer agreement likely reflects the high energetic requirements for photo-fragmentation pathways for these complexes, which is reasonable since they involve elimination of an oxy radical with concomittant reduction of the uranium center. The need to

vibrationally excite the uranyl-anion complexes to a higher level increases the opportunity for the measured ν_3 value to be shifted lower as a result of vibrational anharmonicity, or perhaps by participation of an excited state, as suggested above.

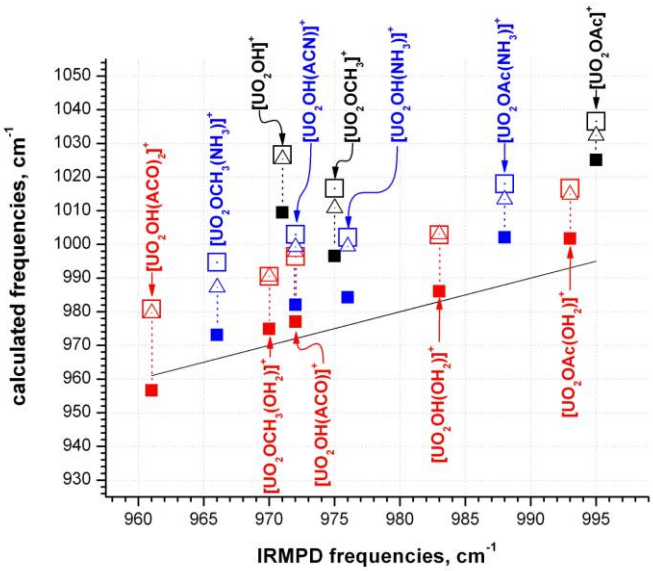

Figure 5. Uranyl ν_3 frequencies calculated using B3LYP plotted versus IRMPD measurements. The line represents the experimental data. Filled square data points were generated using the SDD basis set for all elements, values unscaled. Values represented by open squares were generated using SDD for uranium and 3-21g* for C, H, N and O, while values represented by open triangles utilized 6-31g(d) for C, H, N and O. Black points represent $[UO_2(anion)]^+$ complexes with no neutral donor, red represent those with O-donating neutrals, and blue represent those with N-donating neutrals.

Table 4a. Uranyl antisymmetric stretching frequencies (ν_3) for complexes $[UO_2AS_{0,1,2}]^+$. IRMPD values were generated experimentally, and calculated using the B3LYP functional with various basis sets. All values reported are unscaled.

A (anion)	S (neutral solvent)	IRMPD measure-ments	B3LYP/ SDD/ 3-21g*	B3LYP/ Stuttgart RSC/RLC (SDD)	B3LYP/ Stuttgart RSC/RLC (SDD)/ 6-31+g(d)	B3LYP/ Stuttgart RSC/RLC/ TZVP	B3LYP/ LANL2dz/ aug-cc-pvdz
OH	-	971	1027	1009	1025	1035	988
OH	H_2O	983	1003	986	1003	1015	971
OH	NH_3	976	1002	984	999	1011	964
OH	ACN	972	1003	982	999	--	966
OH	ACO	972	996	977	998	--	961
OH	2 ACO	961	981	957	980	--	945
OAc	-	995	1037	1025	1032	--	993
OAc	H_2O	993	1017	1002	1015	--	985
OAc	NH_3	988	1018	1002	1013	--	976
OCH_3	-	975	1017	997	1011	1018	976
OCH_3	H_2O	970	990	975	990	994	961
OCH_3	NH_3	966	995	973	987	994	959

Table 4b. Uranyl antisymmetric stretching frequencies (ν_3) for complexes $[UO_2AS_{0,1,2}]^+$. IRMPD values were generated experimentally, and calculated using LDA and PW91 functionals with various basis sets. All values reported are unscaled.

A (anion)	S (neutral solvent)	IRMPD measure-ments	LDA/ SVWN/ DNP	LDA/ LANL/ aug-cc-pvdz	LDA/ Stuttgart RSC / TZVP	PW91/ LANL / aug-cc-pvdz	PW91/ Stuttgart RSC / TZVP	ZORA/ PW91/ TZ2P
OH	-	971	995	958	1017	928	987	979
OH	H_2O	983	973	939	1001	910	969	959
OH	NH_3	976	973	937	990	910	962	958
OH	ACN	972	973	--	--	--	--	952
OH	ACO	972	968	--	--	--	--	949
OH	2 ACO	961	939	--	--	--	--	931
OAc	-	995	995	--	--	--	--	987
OAc	H_2O	993	984	--	--	--	--	970
OAc	NH_3	988	986	--	--	--	--	966
OCH_3	-	975	979	949	1003	920	973	964
OCH_3	H_2O	970	961	933	997	904	954	943
OCH_3	NH_3	966	959	932	980	905	950	944

In contrast, calculations using LDA, PW91, and B3LYP/LANL2dz/aug-cc-pVDZ produced unscaled uranyl ν_3 frequencies that were slightly lower than measurements (Figure 6). . The LDA (calculated using DMol[3]) values (Figure 6, open squares) for the $[UO_2A]^+$ complexes and those with a N-donating neutral were in good agreement with measurement, with the salient exception of $[UO_2OH]^+$. Compared to experiments, the LDA values for anion complexes with O-donating ligands were systematically lower

than values for complexes with N-donors, by about 10 cm^{-1}. The value calculated for the $[UO_2OH(ACO)_2]^+$ was ca. 20 cm^{-1} lower than the measured value.

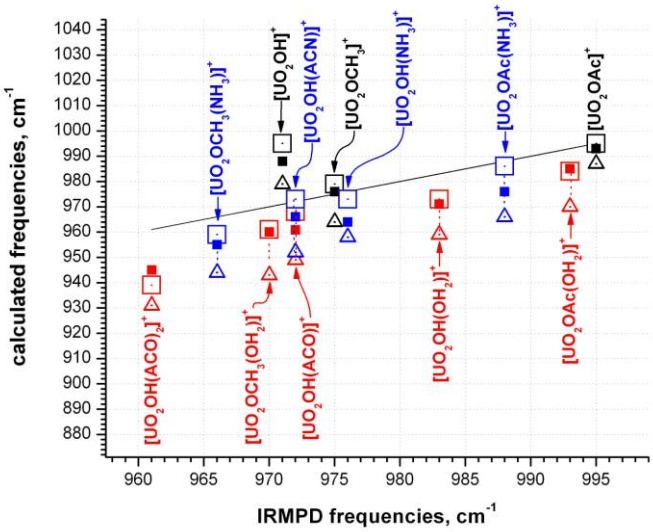

Figure 6. Unscaled uranyl ν_3 frequencies calculated using B3LYP/LANL2dz/aug-cc-pVDZ, LDA/VWN and ZORA/PW91/TZ2P, plotted versus IRMPD measurements. The line represents the experimental data. The open squares were generated using LDA/VWN, the filled squares B3LYP/LANL2dz/aug-cc-pVDZ, and the triangles ZORA/PW91/TZ2P. The black points represent $[UO_2A]^+$ complexes with no neutral donor, red correspond to complexes with O-coordinating neutrals, and blue to those with N-coordinating neutrals.

The values calculated using B3LYP in Figure 6 (filled squares) differed from those in Figure 5 in that they were generated using the LANL2dz/aug-cc-pVDZ basis sets. Values calculated for the uranyl methoxide and acetate complexes without neutrals agreed well with the measured values; the hydroxide species was on the order of 18 cm^{-1} higher. The $[UO_2AS]^+$ complexes were all on the order of 7–15 cm^{-1} lower than the measurements, and there was no apparent systematic difference between the complexes containing O-donors and those with N-donors, which indicated that B3LYP/LANL2dz/aug-cc-pVDZ predicted shifts resulting from both types of ligands consistently.

The frequencies were also computed with ZORA/PW91/TZ2P. The results are consistently lower than the pseudopotential LDA/VWN or B3LYP/LANL2dz/aug-cc-pVDZ values, a feature that was also observed in our earlier work on the neutral donor ligands.[60] The ligand induced shifts are very similar to the results obtained with the other approaches, however, and systematic differences between O- and N-donors were not calculated.

Additional insight into the potential interactions from anion binding can be gained by examining the changes in the calculated bond lengths and angles, which would also check the internal consistency of the predicted stretching frequencies. We selected the calculations performed using B3LYP/SDD/6-31+g** for discussing relationships between calculated bond lengths and frequencies, which are listed in Table 3, and trends in bond lengths with varying ligation are depicted graphically in Figure 7 (detailed structural parameters generated using B3LYP with three different basis sets are contained in Supplementary Tables S1 – S12, and visual representations are provided in Figures 7 - 9). As ligands are added, calculations show that all distances within the uranyl coordination sphere increase. The magnitude of the increase depends not only on the nucleophilic strength of the different ligands but also on their volumes, and the calculations provide a means to develop a more quantitative assessment of the effect of ligand addition to uranyl. The O=U=O bond length is represented by the lower three traces, and the effect of the anion A, and subsequent addition of a neutral solvent S is very similar for the acetate, the hydroxy and the methoxide complexes. The uranyl bond elongates by 0.042 Å, 0.044, and 0.048 Å for OAc^-, OH^- and OCH_3^-, respectively. This is also the order of increasing anion basicity, resulting in donation of more electron density to the uranium atom, and attendant repulsion of the axial oxygen atoms. The amount of donation was quantified by performing charge analysis calculations with ZORA/PW91/TZ2P. The Hirshfeld method shows donation to uranyl of 0.56e (OAc), 0.53e (OH), and 0.65e (OCH_3) while the VDD method gives very similar values of 0.53, 052 and 0.63e, respectively.

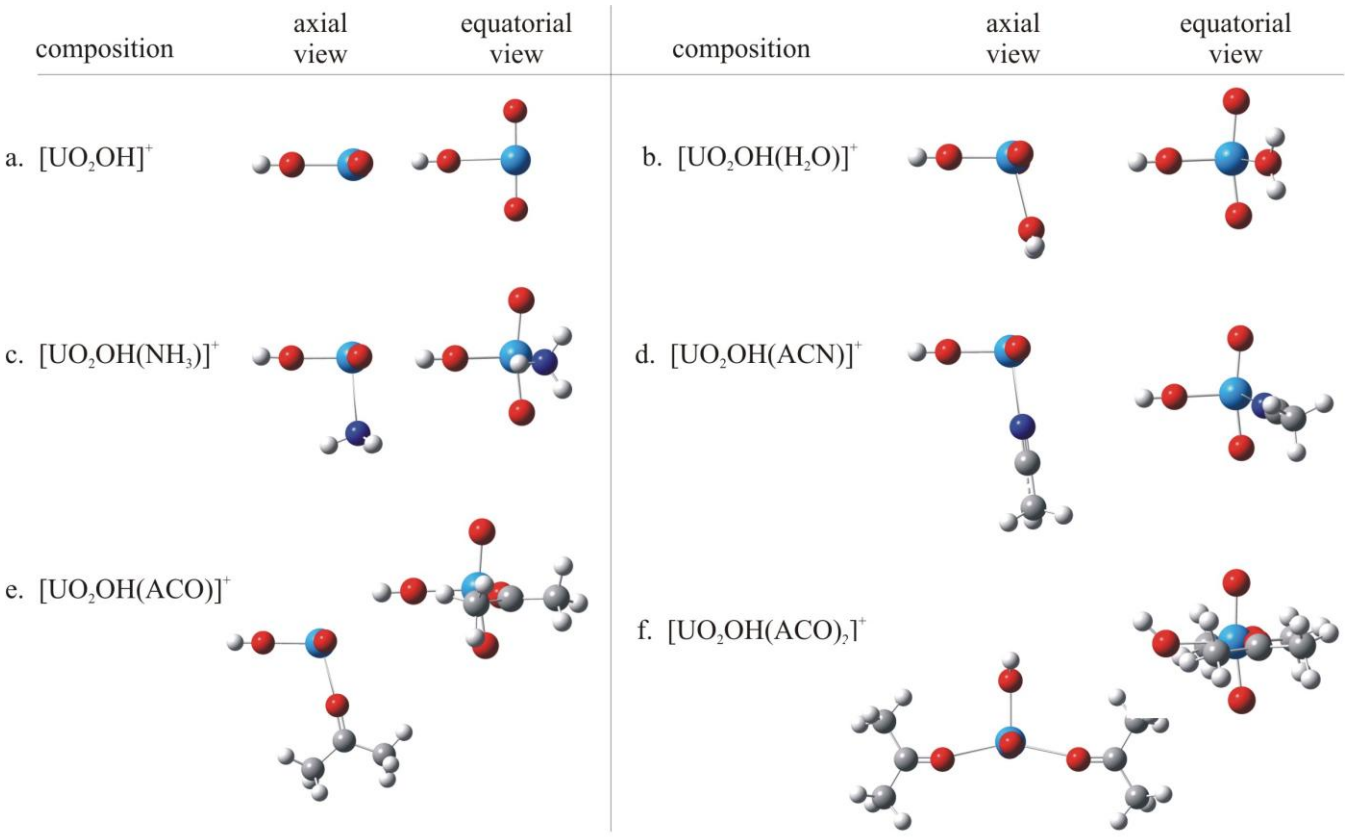

Figure 7. Lowest energy conformations of calculated for $[UO_2OH]^+$ and its solvated complexes. Calculations were performed using hybrid B3LYP functional with the SDD basis set on U and 3-21g* on C, H, N and O.

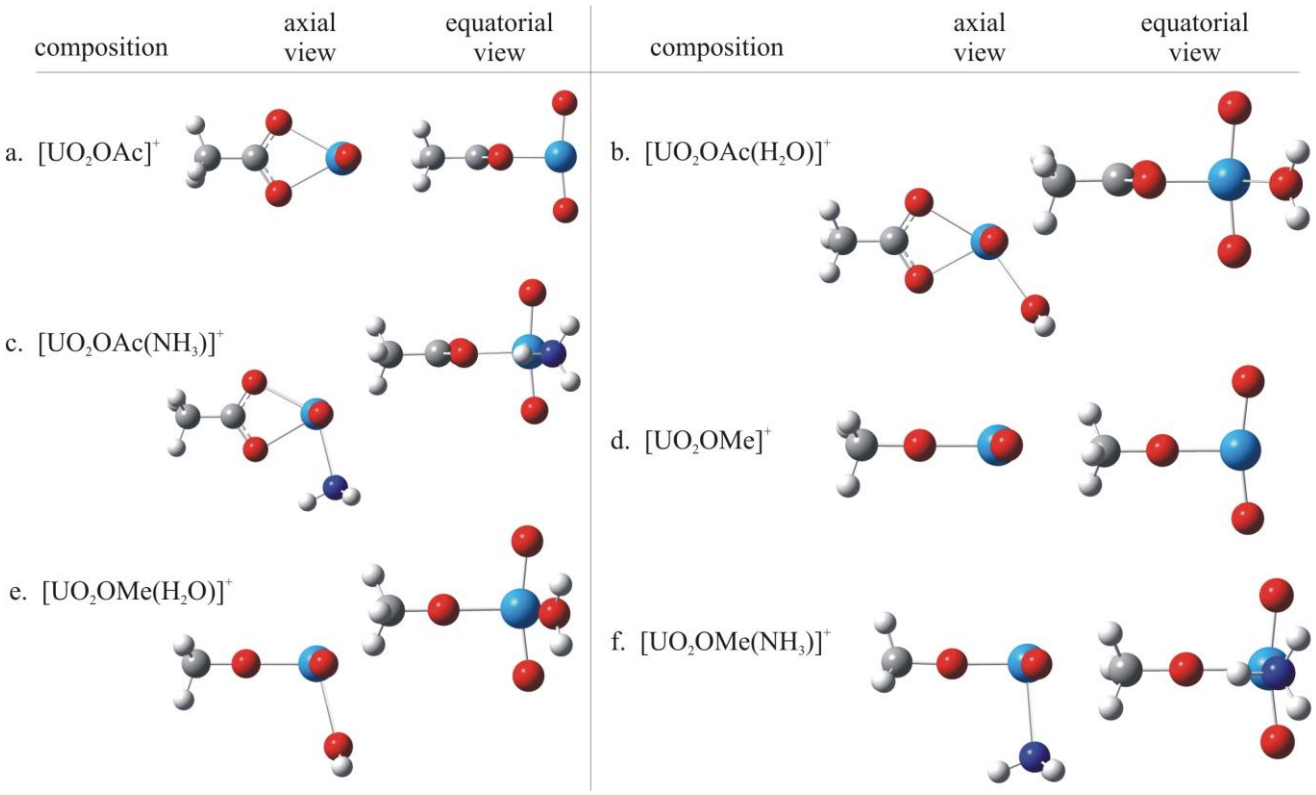

Figure 8. Lowest energy conformations of $[UO_2OAc]^+$, $[UO_2OMe]^+$ and their solvent complexes with water and ammonia. Calculations were performed using hybrid B3LYP functional with the SDD basis set on U and 3-21g* on C, H, N and O.

Table 3. Bond lengths (Angstroms) and O=U=O bond angles for $[UO_2AS]^+$ complexes, calculated using Gaussian 03, at the B3LYP level of theory. The MWB60 (SDD) basis set was used for U, and 3-21g* for C, H, N and O.

A (anion)	S (neutral solvent)	U=O length, Å	U-anion length, Å	U-neutral length, Å	O=U=O angle
$[UO_2]^{2+}$, unligated	n/a	1.7002	n/a	n/a	179.578
OAc	n/a	1.7444	2.2687	n/a	170.346
OAc	H_2O	1.7735	2.2968	2.4616	171.024
OAc	NH_3	1.7540	2.3015	2.5566	171.716
OH	n/a	1.7450	2.0104	n/a	167.409
OH	H_2O	1.7546	2.0277	2.4416	167.606
OH	NH_3	1.7581	2.0332	2.5437	167.245
OH	ACN	1.7571	2.0318	2.4771	166.983
OH	ACO	1.7592	2.0052	2.3252	169.898
OH	$(ACO)_2$	1.7682	2.0828	2.3931	172.640
OCH_3	n/a	1.7510	1.9986	n/a	167.237
OCH_3	H_2O	1.7618	2.0167	2.4514	167.559
OCH_3	NH_3	1.7633	2.0211	2.5561	167.187

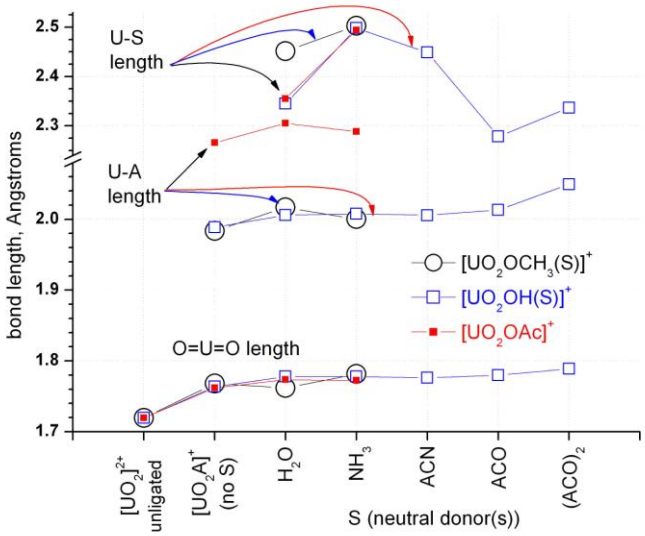

Figure 9. Bond lengths plotted versus neutral for $[UO_2AS]^+$ complexes. Values for unligated $[UO_2]^{2+}$ and $[UO_2A]^+$ complexes are also included. Values were calculated using B3LYP (Gaussian) with the SDD/3-21g* basis set. (Note break in Y axis at 2.08 Å.)

The addition of a neutral donor to the uranyl anion complexes induces a further lengthening of the uranyl bonds (Figure 9), by 0.011 to 0.016 Å, with the largest shifts occurring for the more basic neutrals: in this study addition of ACO caused the largest O=U=O elongation, consistent with the low uranyl frequency measured in the IRMPD spectrum. The magnitude of the elongation on addition of a neutral is much less than that calculated for the initial attachment of the anion. Hirshfeld analysis showed that the strongest donating neutral species, acetone, donates 0.17 e (for one acetone) or 0.25e (for two acetones) to an uranylhydroxide unit in the $[UO_2OH(ACO)_{1,2}]^+$complexes (which have the greatest O=U=O elongation); these values are significantly lower than those calculated for the anions.

The calculations also predict that the uranium-anion distance will be lengthened by addition of a neutral ligand, which is shown by the middle three traces in Figure 9. Increases ranging from 0.017 to 0.024 Å occurred in the U-OH length for the hydroxide complexes, with the magnitude depending on the basicity of the neutral, and the largest elongation being for addition of ACO. When a second ACO is

added, the U-OH distance elongates by another 0.036 Å. The U-OCH_3 bond distance experiences very nearly identical increases upon addition of H_2O and NH_3 to $[UO_2OCH_3]^+$. The U-anion distance calculated for the acetate complex is substantially longer than that for either the hydroxide or the methoxide, and the B3LYP calculations indicated a bidentate-bound acetate, although LDA/VWN suggested a monodentate structure. Using either approach, the U-acetate length is nearly 0.27 Å longer than for the hydroxide or methoxide. Addition of H_2O or NH_3 to the complex causes elongation of the U-acetate bonds by ~ 0.04 and 0.02 Å, respectively. The fact that H_2O produced a longer U-anion elongation than NH_3 is contrary to what would be expected based on calculated coordination energies (NH_3 ~9 kcal/mole greater than H_2O),[40] but may be consistent with the fact that uranyl behaves as a hard acid,[6,40] interacting more strongly with the oxygen donors.

The U-S bond length in $[UO_2AS]^+$ increased when NH_3 was substituted for H_2O, for all three anions studied. Further U-neutral bond length comparisons involved only the hydroxide, and decreased in the order NH_3 > ACN > ACO, minimizing at 2.27 Å. The trend correlates inversely with increasing ligand nucleophilicity. Addition of a second ACO as the third equatorial ligand in $[UO_2OH(ACO)_2]^+$ loosens the overall complex: the U-neutral bond is lengthened by nearly 0.06 Å, and this is accompanied by a lengthening of the U-OH bond by 0.036 Å, and the O=U=O bond by nearly 0.01 Å. As the coordination sphere is completed, distortions of the O=U=O angle from linearity are lessened, and the value approaches 180^o.

CONCLUSIONS

The structure of uranium complexes has been a persistent topic of research in the chemical community because the participation of 5f, 6d and 7s orbitals offers a broad array of possible structures and reaction pathways. The desire to understand and then manipulate uranium chemistry has motivated determined investigations of structure and bonding using spectroscopy and computational chemistry. In principle these approaches should be highly complementary, but in practice results from each cannot be correlated with each other because spectroscopy measurements on condensed phase systems almost always

measure an ensemble of species, while calculations produce data for single discrete species, and do not always include specific and/or long-range interactions with solvent. Consequently it is difficult to use condensed-phase spectroscopic measurements to evaluate computational accuracy, which is badly needed for molecules containing f elements. Infrared spectra of gas phase complexes generated using IRMPD provide data for discrete species that are of great value for evaluating ligand binding trends and computational chemistry results.

Much emphasis has been placed on the study of uranyl dication complexes, and prior IRMPD studies of ACO complexes by our groups enabled comparison of antisymmetric O=U=O and C=O frequencies with solution phase measurements and computational results.[60] However at mid-pH ranges, uranyl-anion pairs are more prevalent and hence in the present study, IRMPD of ion pairs involving hydroxide, acetate and methoxide were examined. The uranyl antisymmetric frequency values were red-shifted equal to or greater than UO_2^{2+} coordinated with four or five neutral donor ligands. While vibrational anharmonicity no doubt contributes to these low frequency values, the intrinsic frequencies of the ion pair complexes are lower than expected when compared with solution phase measurements and with past and present DFT results. The addition of a solvent neutral S to the ion pairs did not result in systematic decreases in the ν_3 values. But when frequencies for the $[UO_2AS]^+$ species were compared for differing neutrals, the ν_3 value decreased with increasing S nucleophilicity, consistent with theory, intuition and previous IRMPD results.[60]

The $[UO_2OCH_3]^+$ molecule underwent wavelength-specific fragmentation reactions, eliminating the OCH_3 radical at a frequency 20 cm^{-1} lower than fragmentations involving rearrangement and or loss of H atom(s). DFT modeling suggested that the OCH_3 radical loss was activated by absorption at the uranyl stretching frequency, while the H atom loss/rearrangement eliminations were activated by absorption at the C-O stretching frequency. Identifying the cause of this phenomenon remains an outstanding task: IRMPD anharmonicity together with absorption non-linearities (as observed in the spectra of the *para*-aminobenzoic acid cation[58] and $[CeOH(ACO)_{n=3,4}]^{2+}$ cation[93]) may contribute to the phenomenon,

however the very large differences in the different photo-fragmentation channels suggests that there may be another factor at work, such as promotion to an excited state electronic configuration, which would be energetically feasible.

ACKNOWLEDGMENTS

Work by G. S. Groenewold and A. K. Gianotto was supported by the U.S. Department of Energy, Assistant Secretary for Environmental Management, and the INL Laboratory Directed Research & Development Program under DOE Idaho Operations Office Contract DE-AC07-05ID14517. M. J. Van Stipdonk was supported in part through a grant from the U. S. National Science Foundation (CAREER-0239800). Gaussian 03 calculations were performed at the Wichita State University High-performance Computing Center (HIPECC), a facility supported by the U. S. National Science Foundation under Grant No. EIA-0216178 and Grant No. EPS-0236913, with matching support from the State of Kansas and HIPECC. W. A. de Jong's research was performed, in part, using the Molecular Science Computing Facility in the William R. Wiley Environmental Molecular Sciences Laboratory, a national scientific user facility sponsored by the U.S. Department of Energy's Office of Biological and Environmental Research located at the Pacific Northwest National Laboratory, which is operated for the Department of Energy by Battelle. The FOM authors, Ivan Infante and Lucas Visscher were supported by the Nederlandse Organisatie voor Wetenschappelijk Onderzoek (Dutch National Science Foundation). The skillful assistance by the FELIX staff, in particular Dr. B. Redlich, is gratefully acknowledged. Construction and shipping of the FTMS instrument was made possible through funding from the National High Field FT-ICR Facility (grant CHE-9909502) at the National High Magnetic Field Laboratory, Tallahassee, FL, as was travel support for one of the INL authors; John Eyler's assistance was particularly invaluable.

SUPPORTING INFORMATION AVAILABLE:

Complete listings of structural data calculated using B3LYP with the SDD, and SDD / 3-21g* basis sets are provided in tables S1–S7 in the supplementary information. Visual representations are also provided, in Figures S1–S4. Complete citations for references 73 and 80 are also included. The material is available free of charge on the Internet at http:\\pubs.acs.org.

REFERENCES

(1) Choppin, G. R.; Rizkalla, E. N. Solution Chemistry of Actinides and Lanthanides. In *Handbook on the Physics and Chemistry of Rare Earths*; Gschneider, J., K. A., Eyring, L., Choppin, G. R., Lander, G. H., Eds.; North-Holland: Amsterdam, 1994; Vol. 18-Lanthanides/Actinides: Chemistry; pp 559.

(2) Denning, R. G. *Struct. Bond.* **1992**, *79*, 215.

(3) Pepper, M.; Bursten, B. E. *Chem. Rev.* **1991**, *91*, 719.

(4) Matsika, S.; Zhang, Z.; Brozell, S. R.; Blaudeau, J.-P.; Wang, Q.; Pitzer, R. M. *J. Phys. Chem. A* **2001**, *105*, 3825.

(5) Silva, R. J.; Nitsche, H. *Radiochim. Acta* **1995**, *70/71*, 377

(6) Morse, J. W.; Choppin, G. R. *Rev. Aquatic Sci.* **1991**, *4*, 1.

(7) Toth, L. M.; Begun, G. M. *J. Phys. Chem.* **1981**, *85*, 547.

(8) Burgess, J. *Metal Ions in Solution*; Ellis Horwood Limited: Chichester, UK, 1978.

(9) Choppin, G. *Radiochim. Acta* **2004**, *92*, 519.

(10) Brookins, D. G. *Geochemical Aspects of Radioactive Waste Disposal*; Springer-Verlag: New York, 1984.

(11) Rizkalla, E. N.; Choppin, G. R. Lanthanides and Actinides Hydration and Hydrolysis. In *Handbook on the Physics and Chemistry of Rare Earths. Volume 18: Lanthanides/Actinides:*

Chemistry; Gschneidner, J., K. A., Eyring, L., Choppin, G. R., Lander, G. H., Eds.; North-Holland: New York, 1994; Vol. 18; pp 529.

(12) Nguyen-Trung, C.; Palmer, D. A.; Begun, G. M.; Peiffert, C.; Mesmer, R. E. *J. Solut. Chem.* **2000**, *29*, 101.

(13) Brooker, M. H.; Huang, C.-H.; Sylwestrowicz, J. *J. Inorg. Nucl. Chem.* **1980**, *42*, 1431.

(14) Glebov, V. A. *Koord. Khim.* **1982**, *8*, 970.

(15) Nguyen-Trung, C.; Begun, G. M.; Palmer, D. A. *Inorg. Chem.* **1992**, *31*, 5280.

(16) Jones, L. H. *Spectrochim. Acta* **1958**, *10*, 395

(17) Quiles, F.; Burneau, A. *Vib. Spectrosc.* **1998**, *18*, 61.

(18) Gal, M.; Goggin, P. L.; Mink, J. *J. Mol. Struct.* **1984**, *114*, 459.

(19) McGlynn, S. P.; Smith, J. K.; Neely, W. C. *J. Chem. Phys.* **1961**, *35*, 105.

(20) Jones, L. H.; Penneman, R. A. *J. Chem. Phys.* **1953**, *21*, 542.

(21) Best, S. P.; Clark, R. J. H.; Cooney, R. P. *Inorg. Chim. Acta* **1988**, *145*, 141.

(22) Clark, D. L.; Conradson, S. D.; Donohoe, R. J.; Keogh, D. W.; Morris, D. E.; Palmer, P. D.; Rogers, R. D.; Tait, C. D. *Inorg. Chem.* **1999**, *38*, 1456.

(23) Kakihana, M.; Nagumo, T.; Okamoto, M.; Kakihana, H. *J. Phys. Chem.* **1987**, *91*, 6128.

(24) Mizuoka, K.; Ikeda, Y. *Radiochim. Acta* **2004**, *92*, 631.

(25) Burns, C. J.; Smith, C. C.; Sattelberger, A. P.; Gray, H. B. *Inorg. Chem.* **1992**, *31*, 3724.

(26) Morris, D. E.; Chisholm-Brause, C. J.; Barr, M. E.; Conradson, S. D.; Gary Eller, P. *Geochim. Cosmochim. Acta* **1994**, *58*, 3613.

(27) Duff, M. C.; Coughlin, J. U.; Hunter, D. B. *Geochim. Cosmochim. Acta* **2002**, *66*, 3533.

(28) Tellez Soto, C. A.; Arissawa, M.; Gomez, L., J.; Mondragon, M. A. *Polyhedron* **2000**, *19*, 2353.

(29) Madic, C.; Hobart, D. E.; Begun, G. M. *Inorg. Chem.* **1983**, *22*, 1494.

(30) Glebov, V. A. *Koord. Khim.* **1981**, *7*, 388.

(31) Mizuoka, K.; Ikeda, Y. *Inorg. Chem.* **2003**, *42*, 3396.

(32) Basile, L. J.; Sullivan, J. C.; Ferraro, J. R.; LaBonville, P. *Appl. Spectrosc.* **1974**, *28*, 142.

(33) Schreckenbach, G.; Hay, P. J.; Martin, R. L. *J. Comput. Chem.* **1999**, *20*, 70.

(34) Vetere, V.; Maldivi, P.; Adamo, C. *J. Comput. Chem.* **2003**, *24*, 850.

(35) Van Wullen, C. *J. Comput. Chem.* **1999**, *20*, 51.

(36) Kaltsoyannis, N. *Chem. Soc. Rev.* **2003**, *32*, 9.

(37) de Jong, W. A.; Harrison, R. J.; Nichols, J. A.; Dixon, D. A. *Theor. Chem. Acc.* **2001**, *107*, 22.

(38) Clavaguera-Sarrio, C.; Ismail, N.; Marsden, C. J.; Begue, D.; Pouchan, C. *Chem. Phys.* **2004**, *302*, 1.

(39) Hay, P. J.; Martin, R. L.; Schreckenbach, G. *J. Phys. Chem. A* **2000**, *104*, 6259.

(40) Clavaguera-Sarrio, C.; Hoyau, S.; Ismail, N.; Marsden, C. J. *J. Phys. Chem. A* **2003**, *107*, 4515.

(41) Farkas, I.; Banyai, I.; Szabo, Z.; Wahlgren, U.; Grenthe, I. *Inorg. Chem.* **2000**, *39*, 799.

(42) Gutowski, K. E.; Dixon, D. A. *J. Phys. Chem. A* **2006**, *110*, 8840.

(43) Gutowski, K. E.; Cocalia, V. A.; Griffin, S. T.; Bridges, N. J.; Dixon, D. A.; Rogers, R. D. *J. Am. Chem. Soc.* **2007**, *129*, 526.

(44) Duncan, M. A. *Int. Rev. Phys. Chem.* **2003**, *22*, 407.

(45) Lemaire, J.; Boissel, P.; Heninger, M.; Mauclaire, G.; Bellec, G.; Mestdagh, H.; Simon, A.; Le Caer, S.; Ortega, J. M.; Glotin, F.; Maitre, P. *Phys. Rev. Lett.* **2002**, *89*.

(46) Moore, D. T.; Oomens, J.; Eyler, J. R.; Meijer, G.; von Helden, G.; Ridge, D. P. *J. Am. Chem. Soc.* **2004**, *126*, 14726.

(47) Oepts, D.; van der Meer, A. F. G.; van Amersfoort, P. W. *Infrared Phys. Technol.* **1995**, *36*, 297.

(48) Fenn, J. B.; Mann, M.; Meng, C. K.; Wong, S. F.; Whitehouse, C. M. *Science* **1989**, *246*, 64.

(49) Schroder, D.; Roithova, J.; Schwarz, H. *Int. J. Mass Spectrom.* **2006**, *254*, 197.

(50) Stewart, I. I. *Spectrochim. Acta, Part B* **1999**, *54*, 1649.

(51) Gatlin, C. L.; Turecek, F. Electrospray Ionization of Inorganic and Organometallic Complexes. In *Electrospray Ionization Mass Spectrometry*; John Wiley & Sons: New York, 1997; pp 527.

(52) Chien, W.; Anbalagan, V.; Zandler, M.; Hanna, D.; Van Stipdonk, M.; Gresham, G.; Groenewold, G. *J. Amer. Soc. Mass Spectrom.* **2004**, *15*, 777.

(53) Van Stipdonk, M.; Anbalagan, V.; Chien, W.; Gresham, G.; Groenewold, G.; Hanna, D. *J. Am. Soc. Mass Spectrom.* e**2003**, *14*, 1205.

(54) Van Stipdonk, M. J.; Chien, W.; Angalaban, V.; Bulleigh, K.; Hanna, D.; Groenewold, G. S. *J. Phys. Chem. A* **2004**, *108*, 10448.

(55) Van Stipdonk, M. J.; Chien, W.; Bulleigh, K.; Wu, Q.; Groenewold, G. S. *J. Phys. Chem. A* **2006**, *110*, 959.

(56) Oomens, J.; Sartakov, B. G.; Meijer, G.; von Helden, G. *Int. J. Mass Spectrom.* **2006**, *254*, 1.

(57) Moore, D. T.; Oomens, J.; van der Meer, L.; von Helden, G.; Meijer, G.; Valle, J.; Marshall, A. G.; Eyler, J. R. *ChemPhysChem* **2004**, *5*, 740.

(58) Oomens, J.; Moore, D. T.; Meijer, G.; von Helden, G. *Phys. Chem. Chem. Phys.* **2004**, *6*, 710.

(59) Oomens, J.; Moore, D. T.; von Helden, G.; Meijer, G.; Dunbar, R. C. *J. Am. Chem. Soc.* **2004**, *126*, 724.

(60) Groenewold, G. S.; Gianotto, A. K.; Cossel, K. C.; Van Stipdonk, M. J.; Moore, D. T.; Polfer, N.; Oomens, J.; de Jong, W. A.; Visscher, L. *J. Am. Chem. Soc.* **2006**, *107*, 4802.

(61) Sachs, S.; Brendler, V.; Geipel, G. *Radiochim. Acta* **2007**, *95*, 103.

(62) Valle, J. J.; Eyler, J. R.; Oomens, J.; Moore, D. T.; van der Meer, A. F. G.; von Helden, G.; Meijer, G.; Hendrickson, C. L.; Marshall, A. G.; Blakney, G. T. *Rev. Sci. Instrum.* **2005**, *76*, 023103.

(63) Marshall, A. G.; Wang, T.-C. L.; Ricca, T. L. *J. Am. Chem. Soc.* **1985**, *107*, 7893.

(64) Bagratashivili, V. N.; Letokov, V. S.; Makarov, A. A.; Ryabov, E. A. *Mutiple Photon Infrared Laser Photophysics and Photochemistry*; Harwood: Chur, Switzerland, 1985.

(65) Oomens, J.; Tielens, A. G. G. M.; Sartakov, B. G.; Von Helden, G.; Meijer, G. *Astrophys. J.* **2003**, *591*, 968.

(66) Marshall, A. G. *Acc. Chem. Res.* **1985**, *18*, 316.

(67) Marshall, A. G.; Hendrickson, C. L.; Jackson, G. S. *Mass Spectrom. Rev.* **1998**, *17*, 1.

(68) Slater, J. C. *Phys. Rev. Lett.* **1951**, *81*, 385.

(69) Vosko, S. J.; Wilk, W.; Nusair, M. *Can. J. Phys.* **1980**, *58*, 1200.

(70) Delley, B. *J. Chem. Phys.* **1990**, *92*, 508.

(71) Delley, B. *J. Chem. Phys.* **2000**, *113*, 7756.

(72) Delley, B. *Int. J. Quantum Chem.* **1998**, *69*, 423.

(73) Becke, A. D. *J. Chem. Phys.* **1993**, *98*, 5648.

(74) Lee, C. T.; Yang, W. T.; Parr, R. G. *Phys. Rev. B* **1988**, *37*, 785.

(75) Aprà, E.; et.al. NWChem, A Computational Chemistry Package for Parallel Computers; Version 4.7 ed.; Pacific Northwest National Laboratory: Richland, Washington 99352-0999, USA, 2005.

(76) Kendall, R. A.; Apra, E.; Bernholdt, D. E.; Bylaska, E. J.; Dupuis, M.; Fann, G. I.; Harrison, R. J.; Ju, J.; Nichols, J. A.; Nieplocha, J.; Straatsma, T. P.; Windus, T. L.; Wong, A. T. *Computer Phys. Comm.* **2000**, *128*, 260.

(77) Frisch, M. J.; Trucks, G. W.; Schlegel, H. B.; Scuseria, G. E.; Robb, M. A.; Cheeseman, J. R.; Zakrzewski, V. G.; Montgomery, J. A. J.; Stratmann, R. E.; Burant, J. C.; Dapprich, S.; Millam, J.

M.; Daniels, A. D.; Kudin, K. N.; Strain, M. C.; Farkas, O.; Tomasi, J.; Barone, V.; Cossi, M.; Cammi, R.; Mennucci, B.; Pomelli, C.; Adamo, C.; Clifford, S.; Ochterski, J.; Petersson, G. A.; Ayala, P. Y.; Cui, Q.; Morokuma, K.; Malick, D. K.; Rabuck, A. D.; Raghavachari, K.; Foresman, J. B.; Cioslowski, J.; Ortiz, J. V.; Stefanov, B. B.; Liu, G.; Liashenko, A.; Piskorz, P.; Komaromi, I.; Gomperts, R.; Martin, R. L.; Fox, D. J.; Keith, T.; Al-Laham, M. A.; Peng, C. Y.; Nanayakkara, A.; Gonzalez, C.; Challacombe, M.; Gill, P. M. W.; Johnson, B.; Chen, W.; Wong, M. W.; Andres, J. L.; Gonzalez, C.; Head-Gordon, M.; Replogle, E. S.; Pople, J. A. Gaussion 98, Revision A.4; Gaussian, Inc.. Pittsburgh, PA, 1998.

(78) Ortiz, J. V.; Hay, P. J.; Martin, R. L. *J. Am. Chem. Soc.* **1992**, *114*, 2736.

(79) Dunning, T. H. *J. Chem. Phys.* **1989**, *90*, 1007.

(80) Chaban, G. M.; Jung, J. O.; Gerber, R. B. *J. Chem. Phys.* **1999**, *111*, 1823.

(81) Matsunaga, N.; Chaban, G. M.; Gerber, R. B. *J. Chem. Phys.* **2002**, *117*, 3541.

(82) Yagi, K.; Hirao, K.; Taketsugu, T.; Schmidt, M. W.; Gordon, M. S. *J. Chem. Phys.* **2004**, *121*, 1383.

(83) Bergner, A.; Dolg, M.; Kuchle, W.; Stoll, H.; Preuss, H. *Mol. Phys.* **1993**, *80*, 1431.

(84) Dolg, M. *Modern Methods and Algorithms of Quantum Chemistry*; John von Neumann Institute for Computing: Julich, Germany, 2000; Vol. 1.

(85) Dunning, T. H., Jr.; Hay, P. H. *Modern Theoretical Chemistry*; Plenum: New York, 1976; Vol. 3.

(86) Kuchle, W.; Dolg, M.; Stoll, H.; Preuss, H. *Mol. Phys.* **1991**, *74*, 1245.

(87) te Velde, G.; Bickelhaupt, F. M.; Baerends, E. J.; Guerra, C. F.; Van Gisbergen, S. J. A.; Snijders, J. G.; Ziegler, T. *J. Comput. Chem.* **2001**, *22*, 931.

(88) van Lenthe, E.; Baerends, E. J.; Snijders, J. G. *J. Chem. Phys.* **1993**, *99*, 4597.

(89) Perdew, J. P.; Chevary, J. A.; Vosko, S. H.; Jackson, K. A.; Pederson, M. R.; Singh, D. J.; Fiolhais, C. **1992**, *46*, 6671.

(90) Soderholm, L.; Skanthakumar, S.; Neuefeind, J. *Anal. Bioanal. Chem.* **2005**, *383*, 48.

(91) Neuefeind, J.; Soderholm, L.; Skanthakumar, S. *J. Phys. Chem. A* **2004**, *108*, 2733.

(92) Quiles, F.; Burneau, A. *Vib. Spectrosc.* **2000**, *23*, 231.

(93) Groenewold, G. S.; Gianotto, A. K.; Cossel, K. C.; Van Stipdonk, M. J.; Oomens, J.; Polfer, N.; Moore, D. T.; de Jong, W. A.; McIlwain, M. E. *Phys. Chem. Chem. Phys.* **2006**, *9*, 596.

(94) Kasha, M. *J. Chem. Phys.* **1949**, *17*, 349.

(95) Lias, S. G. NIST Chemistry WebBook; United States Department of Commerce, National Institute of Standards and Technology, 2003; Vol. 2004.

(96) de Jong, W. A.; Apra, E.; Windus, T. L.; Nichols, J. A.; Harrison, R. J.; Gutowski, K. E.; Dixon, D. A. *J. Phys. Chem. A* **2005**, *109*, 11568.

(97) Rodgers, M. T.; Armentrout, P. B. *Mass Spectrom. Rev.* **2000**, *19*, 215.

(98) Banisaukas, J.; Szczepanski, J.; Eyler, J. R.; Vala, M.; Hirata, S.; Head-Gordon, M.; Oomens, J.; Meijer, G.; von Helden, G. *J. Phys. Chem. A* **2003**, *107*, 782.

(99) Fielicke, A.; Mitric, R.; Meijer, G.; Bonacic-Koutecky, V.; von Helden, G. *J. Am. Chem. Soc.* **2003**, *125*, 15716.

(100) Forsman, J. B.; Frisch, A. E. *Exploring Chemistry with Electronic Structure Methods*, 2nd ed.; Gaussian: Pittsburgh, PA, 1996.

(101) Langhoff, S. R. *J. Phys. Chem.* **1996**, *100*, 2819.

SUPPLEMENTARY INFORMATION

Infrared Spectroscopy Discrete Uranyl Anion Complexes

Gary S. Groenewold,* Anita K. Gianotto, Michael E. McIlwain, Michael J. Van Stipdonk,* Michael Kullman, Travis J. Cooper, David T. Moore, Nick Polfer, Jos Oomens, Ivan Infante, Lucas Visscher, Bertrand Siboulet, and Wibe A. de Jong

Table S1. Unscaled frequencies for $[UO_2]^{2+}$ and $[UO_2A]^{+}$ complexes, calculated using B3LYP and the SDD (MWB60) basis set for all atoms.

A (anion)	Antisymmetric O=U=O Stretch (ν_3), cm^{-1}	Symmetric O=U=O Stretch (ν_1), cm^{-1}	Other
$[UO_2]^{2+}$	1120.30	-	157.42
OAc	1025.08	936.23	-
OH	1009.46	926.75	701.70 (U-O)
OCH_3	996.53	905.71	1029.72 (O-CH_3)

Table S2. Unscaled frequencies for $[UO_2AS]^+$ complexes. calculated using calculated using B3LYP and the SDD (MWB60) basis set for all atoms.

A (anion)	S (neutral)	Antisymmetric O=U=O Stretch (ν_3), cm^{-1}	Symmetric O=U=O Stretch (ν_1), cm^{-1}	Other
OH	H_2O	986.06	905.13	683.38 (U-OH)
	NH_3	984.23	903.71	685.28 (U-OH)
	ACN			
	ACO	977.01	896.07	666.76 (U-OH)
	$(ACO)_2$	956.65	-	638.17 (U-OH)
OCH_3	H_2O	974.85	886.98	1054.48
	NH_3	973.09	885.89	1056.86
OAc	H_2O	1001.69	914.06	-
	NH_3	1002.08	914.76	-

Table S3. Bond lengths (Angstroms) and O=U=O bond angles for $[UO_2]^{2+}$ and $[UO_2A]^+$ complexes. calculated using B3LYP and the SDD (MWB60) basis set for all atoms.

A (anion)	U=O length, Å	U-O length (U to anion), Å	O=U=O angle
$[UO_2]^{2+}$ unligated	1.7167	-	180.0
OAc	1.7609	2.2705	169.656
OH	1.7630	2.0008	166.912
OCH_3	1.7685	1.9915	166.611

Table S4. Bond lengths (Angstroms) and O=U=O bond angles for $[UO_2AS]^+$ complexes. calculated using B3LYP and the SDD (MWB60) basis set for all atoms.

A (anion)	S (neutral)	U=O length, Å	U-anion length, Å	U-ligand length, Å	O=U=O angle
OH	H_2O	1.7763	2.0197	2.3869	166.982
	NH_3	1.7773	2.0237	2.5085	166.566
	ACN				
	ACO	1.7795	2.0303	2.2863	167.059
	$(ACO)_2$	1.7899	2.0556	2.3510	169.423
OCH_3	H_2O	1.7814	2.0099	2.3954	166.803
	NH_3	1.7822	2.0134	2.5183	166.374
OAc	H_2O	1.7718	2.3185	2.3978	170.367
	NH_3	1.7713	2.3027	2.5104	170.651

Table S5. Unscaled frequencies for $[UO_2]^{2+}$ and $[UO_2A]^{+}$ complexes, calculated using B3LYP with the SDD (MWB60) basis set for U, and 3-21g* for C, H, N and O.

A (anion)	Antisymmetric O=U=O stretch (ν_3), cm^{-1}	Symmetric O=U=O stretch (ν_1), cm^{-1}	Other
$[UO_2]^{2+}$	1124.69	-	183.27 (U-O)
OAc	1036.514	945.49	-
OH	1026.58	941.42	734.61 (U-O)
OCH_3	1016.62	922.96	1041.61 (O-CH3)

Table S6. Unscaled frequencies for $[UO_2AS]^{+}$ complexes, calculated using B3LYP with the SDD (MWB60) basis set for U, and 3-21g* for C, H, N and O.

A (anion)	S (neutral)	Antisymmetric O=U=O stretch (ν_3), cm^{-1}	Symmetric O=U=O stretch (ν_1), cm^{-1}	Other
OH	H_2O	1002.78	919.82	715.99 (U-OH)
	NH_3	1002.03	919.38	717.72 (U-OH)
	ACN	1002.93	919.29	714.40 (U-OH)
	ACO	996.34	913.06	705.59 (U-OH)
	$(ACO)_2$	980.77	897.11	666.29 (U-OH)
OCH_3	H_2O	990.49	905.25	1079.62 (U-OCH_3)
	NH_3	994.66	904.73	1067.07 (U-OCH_3)
OAc	H_2O	1016.66	927.48	-
	NH_3	1017.97	928.55	-

Table S7. Bond lengths (Angstroms) and O=U=O bond angles for $[UO_2]^{2+}$ and $[UO_2A]^{+}$ complexes, calculated using B3LYP with the SDD (MWB60) basis set for U, and 3-21g* for C, H, N and O.

A (anion)	U=O length, Å	U-O length (U to ligand), Å	O=U=O angle
$[UO_2]^{2+}$ unligated	1.7193	-	180.000
OAc	1.7617	2.2658	170.628
OH	1.7636	1.9887	167.618
OCH_3	1.7681	1.9835	167.555

Table S8. Bond lengths (Angstroms) and O=U=O bond angles for $[UO_2AS]^{+}$ complexes, calculated using B3LYP with the SDD (MWB60) basis set for U, and 3-21g* for C, H, N and O.

A (anion)	S (neutral)	U=O length, Å	U-anion length, Å	U-ligand length, Å	O=U=O angle
OH	H_2O	1.7778	2.0060	2.3450	168.121
	NH_3	1.7780	2.0078	2.4979	167.681
	ACN	1.7762	2.0056	2.4486	167.422
	ACO	1.7797	2.0133	2.2784	168.146
	$(ACO)_2$	1.7890	2.0493	2.3368	172.843
OCH_3	H_2O	1.7618	2.0167	2.4514	167.559
	NH_3	1.7814	2.0004	2.5031	167.652
OAc	H_2O	1.7735	2.3050	2.3552	171.450
	NH_3	1.7723	2.2884	2.4942	171.715

Table S9. Unscaled frequencies for $[UO_2]^{2+}$ and $[UO_2A]^{+}$ complexes, calculated using B3LYP with the SDD (MWB60) basis set for U, and 6-31+g** for C, H, N and O.

A (anion)	Antisymmetric O=U=O stretch (ν_3), cm^{-1}	Symmetric O=U=O stretch (ν_1), cm^{-1}	Other
$[UO_2]^{2+}$	1140.17	-	183.41 (U-O)
OAc	1032.31	949.82	-
OH	1025.38	945.98	678.71 (U-O)
OCH_3	1010.81	923.05	1054.43 (O-CH_3)

Table S10. Unscaled frequencies for $[UO_2AS]^{+}$ complexes, calculated using B3LYP with the SDD (MWB60) basis set for U, and 6-31+g** for C, H, N and O.

A (anion)	S (neutral)	Antisymmetric O=U=O stretch (ν_3), cm^{-1}	Symmetric O=U=O stretch (ν_1), cm^{-1}	Other
OH	H_2O	1003.05	925.22	658.56 (U-OH)
	NH_3	999.39	922.3	656.09 (U-OH)
	ACN	999.23	921.31	652.34 (U-OH)
	ACO	997.79	917.85	626.43 (U-OH)
	$(ACO)_2$	979.63	900.29	592.51 (U-OH)
OCH_3	H_2O	990.49	905.25	1079.62 (U-OCH_3)
	NH_3	987.23	902.94	1080.10 (U-OCH_3)
OAc	H_2O	1014.81	925.96	-
	NH_3	1013.37	926.16	-

Table S11. Bond lengths (Angstroms) and O=U=O bond angles for $[UO_2]^{2+}$ and $[UO_2A]^{+}$ complexes, calculated using B3LYP with the SDD (MWB60) basis set for U, and 6-31+g** for C, H, N and O.

A (anion)	U=O length, Å	U-O length (U to ligand), Å	O=U=O angle
$[UO_2]^{2+}$ unligated	1.7002	-	179.578
OAc	1.7450	2.0104	167.409
OH	1.7510	1.9986	167.237
OCH_3	1.7681	1.9835	167.555

Table S12. Bond lengths (Angstroms) and O=U=O bond angles for $[UO_2AS]^{+}$ complexes, calculated using B3LYP with the SDD (MWB60) basis set for U, and 6-31+g** for C, H, N and O.

A (anion)	S (neutral)	U=O length, Å	U-anion length, Å	U-ligand length, Å	O=U=O angle
OH	H_2O	1.7546	2.0277	2.4416	167.606
	NH_3	1.7581	2.0332	2.5437	167.245
	ACN	1.7571	2.0318	2.4771	166.983
	ACO	1.7592	2.0052	2.3252	169.898
	$(ACO)_2$	1.7682	2.0828	2.3931	172.640
OCH_3	H_2O	1.7618	2.0167	2.4514	167.559
	NH_3	1.7633	2.0211	2.5561	167.187
OAc	H_2O	1.7735	2.2968	2.4616	171.024
	NH_3	1.7540	2.3015	2.5566	171.716

Complete citation information for references found in document with more than 10 authors.

73) Aprà, E.; Windus, T. L.; Straatsma, T. P.; Bylaska, E. J.; de Jong, W.; Hirata, S.; Valiev, M.; Hackler, M.; Pollack, L.; Kowalski, K.; Harrison, R.; Dupuis, M.; Smith, D. M. A.; Nieplocha, J.; V., T.; Krishnan, M.; Auer, A. A.; Brown, E.; Cisneros, G.; Fann, G.; Fruchtl, H.; Garza, J.; Hirao, K.; Kendall, R.; Nichols, J.; Tsemekhman, K.; Wolinski, K.; Anchell, J.; Bernholdt, D.; Borowski, P.; Clark, T.; Clerc, D.; Dachsel, H.; Deegan, M.; Dyall, K.; Elwood, D.; Glendening, E.; Gutowski, M.; Hess, A.; Jaffe, J.; Johnson, B.; Ju, J.; Kobayashi, R.; Kutteh, R.; Lin, Z.; Littlefield, R.; Long, X.; Meng, B.; Nakajima, T.; Niu, S.; Rosing, M.; Sandrone, G.; Stave, M.; Taylor, H.; Thomas, G.; van Lenthe, J.; Wong, A.; Zhang, Z.; Version 4.7 ed.; Pacific Northwest National Laboratory: Richland, Washington 99352-0999, USA, 2005

80) Frisch, M. J.; Trucks, G. W.; Schlegel, H. B.; Scuseria, G. E.; Robb, M. A.; Cheeseman, J. R.; Zakrzewski, V. G.; Montgomery, J. A. J.; Stratmann, R. E.; Burant, J. C.; Dapprich, S.; Millam, J. M.; Daniels, A. D.; Kudin, K. N.; Strain, M. C.; Farkas, O.; Tomasi, J.; Barone, V.; Cossi, M.; Cammi, R.; Mennucci, B.; Pomelli, C.; Adamo, C.; Clifford, S.; Ochterski, J.; Petersson, G. A.; Ayala, P. Y.; Cui, Q.; Morokuma, K.; Malick, D. K.; Rabuck, A. D.; Raghavachari, K.; Foresman, J. B.; Cioslowski, J.; Ortiz, J. V.; Stefanov, B. B.; Liu, G.; Liashenko, A.; Piskorz, P.; Komaromi, I.; Gomperts, R.; Martin, R. L.; Fox, D. J.; Keith, T.; Al-Laham, M. A.; Peng, C. Y.; Nanayakkara, A.; Gonzalez, C.; Challacombe, M.; Gill, P. M. W.; Johnson, B.; Chen, W.; Wong, M. W.; Andres, J. L.; Gonzalez, C.; Head-Gordon, M.; Replogle, E. S.; Pople, J. A. *Gaussion 98, Revision A.4*, Gaussian, Inc.. Pittsburgh, PA, 1998.